Summer 2019

A Design of Inductive Coupling Wireless Power Transfer System for Electric Vehicle Applications

Sarika Reddy Daida
Old Dominion University, daidasarikareddy@gmail.com

Recommended Citation

A DESIGN OF INDUCTIVE COUPLING WIRELESS POWER TRANSFER

SYSTEM FOR ELECTRIC VEHICLE APPLICATIONS

by

Sarika Reddy Daida
B.E. May 2016, Jawaharlal Nehru Technological University, India

A Thesis Submitted to the Faculty of
Old Dominion University in Partial Fulfillment of the
Requirements for the Degree of

MASTER OF SCIENCE

ELECTRICAL AND COMPUTER ENGINEERING

OLD DOMINION UNIVERSITY
August 2019

Approved by:

Yucheng Zhang (Director)

Shirshak Dhali (Member)

Shu Xiao (Member)

ABSTRACT

A DESIGN OF INDUCTIVE COUPLING WIRELESS POWER TRANSFER SYSTEM FOR
ELECTRIC VEHICLE APPLICATIONS

Daida Sarika Reddy
Old Dominion University, 2019
Director: Dr. Yucheng Zhang

This research focuses on the study of using an inductive-coupled Wireless Power Transfer (WPT) system for electric vehicle charging applications in Medium Voltage DC (MVDC) power networks. Implementing WPT in Electric Vehicles (EVs) can provide a convenient alternative charging option, versus static charging in a station that would take hours. Also, it can prevent the potential of electrocution hazards that might occur due to the usage of physical medium like wires in EV charging. Even though inductive coupling has been applied in some applications of WPT, it is still not efficient enough to transfer high power at the kilowatts level due to weak coupling between the transmitter and the receiver. Using optimally-specified resonant circuits along with inductive coupling can enhance the coupling and make the system more efficient for practical applications.

This research aims to design and analyze the performance of a 5-KW WPT circuit. The optimal specification of a resonant circuit is studied and discussed. Theoretical calculations are performed to find the component values in the circuit to reach. The WPT system is firstly verified by performing simulation tests in the MATLAB/SIMULINK environment and then on a low power hardware testbed.

This thesis is dedicated to my parents, my brother Ravi for believing in me and providing me with everything I need. And to my advisor for his patience in supporting me throughout my thesis work.

ACKNOWLEDGEMENTS

I extend many, many thanks to Dr. Yucheng Zhang, my advisor for his patience, support and valuable guidance throughout my thesis work. His guidance and support have always been very helpful for the development of my thesis.

I am grateful to my committee members Dr. Shu Xiao and Dr. Shirshak Dhali for spending their time on giving valuable suggestions.

Special thanks to the Graduate Program Director, Chunsheng Xin for helping me in making the degree plan and guiding me throughout my master's program.

I would like to thank Yashwanth Bezwada and Sagar Bhatta for helping me whenever needed while dealing with the hardware in the lab.

I would like to thank staff of Electrical and Computer Engineering at Old Dominion University, including Romina Samson and Lori Barrett for their immense help in every semester.

I also thank my family and friends for their unconditional love, support and encouragement throughout.

NOMENCLATURE

AC	Alternating Current
DC	Direct Current
WPT	Wireless power transfer
EV	Electric Vehicle
ICE	Internal Combustion Engine
MVDC	Medium Voltage Direct Current
IPT	Inductive Power Transfer
CPT	Capacitive Power Transfer
HEV	Hybrid Electric Vehicle
PHEV	Plug in Hybrid Electric Vehicle
PWM	Pulse Width Modulation
MOSFET	Metal oxide semiconductor field effect Transistor

TABLE OF CONTENTS

LIST OF TABLES

Table   Page

LIST OF FIGURES

CHAPTER 1

INTRODUCTION

1.1 Introduction

Since a few decades ago, the use of Electric Vehicles (EVs) has increased due to the advantages they possess when compared to Internal Combustion Engine (ICE) vehicles. The former have much less carbon emission, which prevents global warming to a considerable extent. Since the invention of EVs, they have gone through many stages of transformation in terms of their design topology and in-built technology. The aim of this thesis is to design and analyze an inductive coupled wireless power transfer (WPT) topology for EVs to integrate with Medium Voltage DC (MVDC) networks. The main focus of the design will be on studying and analyzing a resonant circuit topology to apply to the wireless inductive power transfer (IPT) design.

With the present pace in the development of technology and urbanization, the number of personal vehicles is expected to increase. As most of the vehicles being used presently depend on fossil fuels, one can estimate the issues the usage of oil can bring to humanity. It can lead to global climate change, poor air quality and few political conflicts. Presently, the world is using nearly 85 million barrels of oil every day. 60% of the total oil is being used for transportation out of which 25% is consumed by the United States. It is proven that only 1300 billion barrels is available for further usage, which can lead to the scarcity of oil after 40 years. In preventing this EVs can play a major role as they are clean and secure [1].

Even though EVs are challenging conventional ICE vehicles in terms of energy efficiency and long term sustainability, the usage of physical medium for the transmission of power can sometimes be hazardous. In fact, EVs were invented many years ago in 1895, but there were many

factors that influenced the EV market that led to the downfall of EVs in 1930. Some of those major factors are listed below.

1) The charging time for EVs was nearly 8 hours or more, which is very long. The cost of EVs was 40% more compared to ICE vehicles.

2) Besides buying an EV, operating and maintenance costs were high compared to ICE vehicles.

3) Even though there was no proof that EVs are less safe compared to ICE vehicles, automobile manufacturers hesitated to spend money in research, development and manufacturing of EVs as there was a downfall in the market by that time.

4) In the 1990s lead acid batteries were used in most of EVs which made the vehicle very heavy and required a long battery charging time. Also, there was no good infrastructure to recharge EVs.

5) Even the prices of hybrid electric vehicles (HEVs) and Plug in Hybrid Electric Vehicles (PHEVs) were higher compared to gasoline based ones.

Even in recent times, EVs suffer the drawbacks caused due to energy storage technologies. Batteries have unsatisfactory energy densities, a shorter lifetime and higher costs. For example, the expansion of a traditional transit electric bus is tough because of the battery size and cost. The battery in a bus can weigh 26% of the total weight of the bus, and it can cost up to 39% of the total cost [2]. Designing a battery with high energy density, high power density, proper safety and reliability is not an easy task. Moreover, charging the vehicle a single time may take half an hour to many hours, depending on the power level of the charger. To overcome this, batteries with fast charging capabilities were proposed, but these batteries need high charge acceptance and are not ideal for use in a vehicle. Also, it may lead to increased chances of electric shock in harsh weather

conditions. Because of all these disadvantages, EV owners are showing interest towards WPT vehicles. Wireless charging can make the task easier and reduce battery size [3,4].

1.2 MVDC Networks

Besides AC distribution networks, Medium Voltage DC (MVDC) networks are now considered as a new technology capable of increasing power quality and transfer capacity in distribution systems. These systems possess a few advantages compared to the ac grid infrastructures. In the MVDC distribution networks, power transmission capacity can be increased as no reactive current will be carried. Also, MVDC needs fewer materials and overcomes the disadvantage of installing bulky devices like transformers for power conversion. The medium voltage level of these systems has lower currents leading to lower conduction losses [5,6]. An increased interest is being shown in MVDC systems due to the expansion of the energy market, which led to a large number of wind and solar power plant installations. The present expansion rate of these technologies in the United States will require a dc integration link to improve efficiency and system performance, which can happen with MVDC networks [7]. These advantages are making MVDC systems fall into the focus of practical and theoretical research projects [8,9].

In [10] it is stated that most of the loads that are being served by AC power grids are DC type. Nearly 80% of the loads in the commercial sector and residential houses are DC [11], so integrating MVDC networks into the power supply systems can reduce DC-AC-DC conversion losses leading to low energy consumption in the circuitry. In this thesis model, the integration of EVs to MVDC networks can assist the EV model in reducing these losses. The current existing EV charging stations, depend on AC chargers that require a two stage AC-DC-AC conversion process on the

transmitting side. As the resonant circuit needs high frequencies, conversion of low frequency AC supply to DC is done by a rectifier and then DC is converted to AC again with high frequency using an inverter. Besides the above mentioned advantages MVDC networks possess, they can also eliminate this two stage conversion process in the EV, so having EV systems directly tied to the MVDC architecture can improve system efficiency by reducing the power conversion stages.

1.3 WPT Technologies

WPT was first introduced by Nikola Tesla who carried out various experiments on WPT in Colorado Springs, USA in the 1890s [12]. To carry the energy between the transmitter and receiver, air medium is used by WPT which is energized by charged particles. Depending on the applications, power ratings and the range of transmission, the energy can be transferred through an electric field, a magnetic field or electromagnetic waves. Depending on the distance the WPT techniques are divided into near field and far field as shown in Fig 1. When the energy is to be transferred through shorter distances, near field methods are used; when it is to be transmitted for longer distances far field techniques are used.

Recently microwave beamforming, one of the methods of the far field technique, was used in EVs and PHEVs. In [13], a model was proposed that uses a roadside transmitter to power the EV with 80% RF-DC conversion efficiency. In the last 10 years this technique has been used in medium power applications, such as recharging portable electronic devices. However, the electromagnetic fields involved in the far field technologies are stronger when compared to the near field, which makes near field transmission safer for humans [14-16]. Taking this into account, the design of this system model adopts Inductive power transfer (IPT) method in WPT which falls into the category of near field transmission. Even though near field systems have limitations related

to transmission range, lower data rates and sensitivity with respect to the positions of the transmitter and receiver, these factors may not affect the performance in existing applications which require only low data rates for short distances. A few researchers stated that these systems can also be advantageous in terms of attaining security [17].
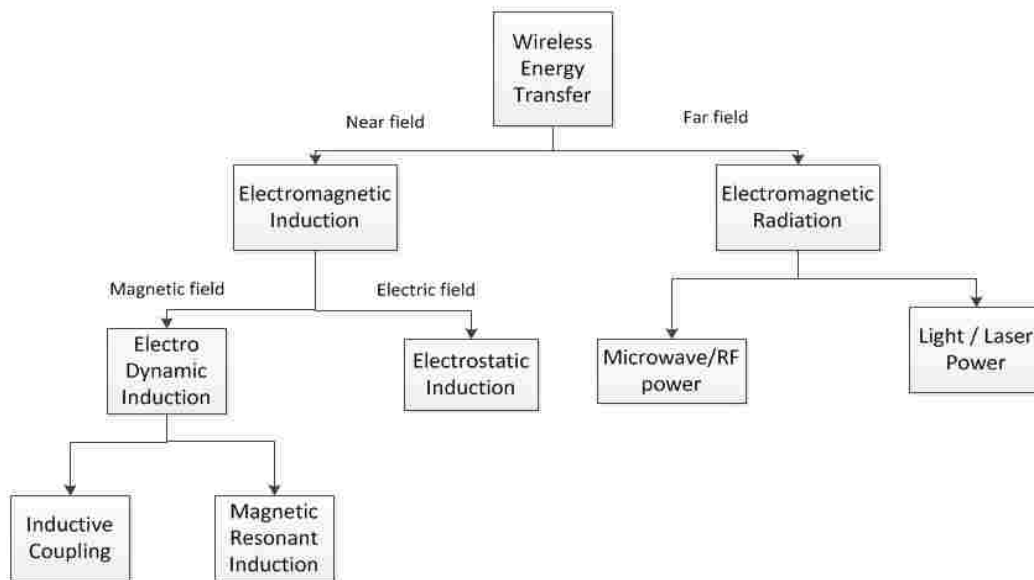
Fig 1: Examples of energy transfer in near field and far field

Nowadays, due to the advantages WPT possesses, it is used in most mobile devices, electric vehicles, home appliances [18]. It is also used in Solar power satellites and defense systems.

1.4 Inductive power transfer

In the near field transmission there are two primarily used techniques that are being applied in the present practical applications which can be categorized based on the coupling technology used in them. These coupling techniques are listed below.

1) Inductive coupling

2) Capacitive coupling.

Inductive coupling is one of the near field transmission techniques, in which the energy transfer is done between the two coils through magnetic fields. The coils will be placed in close proximity for transmission from transmitter to receiver. The mutual induction principle is used to transfer the energy between the two coils without using any physical medium. When a current is passed through the transmitter coil, it will produce a magnetic field in short range. When the receiver coil is brought and placed in this field, the current or voltage will be induced in the receiver coil. This induced voltage can be used for charging a device which is wireless or a storage system. In this way the electrical power is transferred from one coil to the other coil using the magnetic field. Because of mutual induction, the energy will be transferred between the coils in inductive coupling. A basic outline of inductive coupling is shown in Fig 2.A transformer can be a best example to explain how mutual induction works in which there will not be any contact between the primary and secondary coils.

Inductive power transfer can handle many kinds of power loads without major problems and with greater efficiency, and it is being used in a wide range of near field applications as it can retain greater efficiency within a meter [19]. The mutual position and the distance of the transmitter and receiver plays a role in deciding the accuracy of transmission. However, this technique works well only for limited, short distances. When the distance is increased between the coils, or the secondary coil is placed apart from the primary coil, the amount of power transfer will be decreased. The application of inductive coupling for power transmission through longer distances is still under development [20]. As in the case of inductive coupling, capacitive coupling is also primarily used for shorter distances, but the transfer of power is done through electric fields.
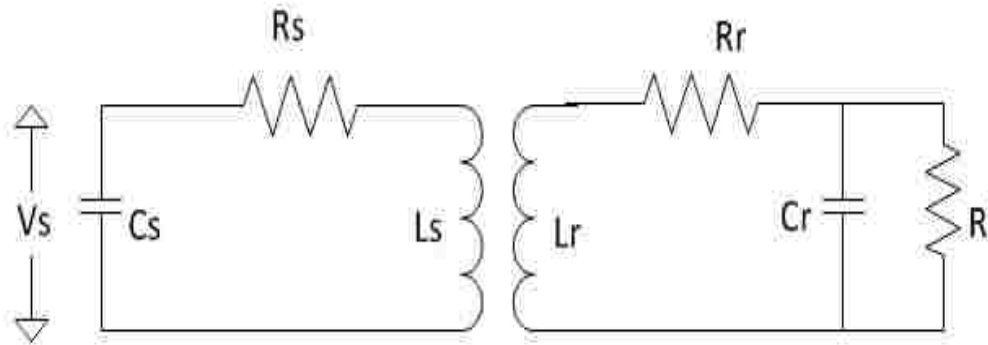
Fig 2: Transformer or Inductive coupling.

Even though both of these coupling techniques can be used for power transfer in EVs, this model uses inductive coupling due to its advantages compared to capacitive coupling. Some of the advantages of inductive coupling over capacitive coupling are:

1) CPT, although it is developing in small gap applications, is limited to low power level transmissions over short distances while IPT can be used for both low power to high power levels. CPT is suitable for gaps smaller than 1mm, while IPT is being applied in applications that require power transfer in centimeters, like in the case of EVs, factories, industrial automotive applications. [20]

2) As IPT deals with magnetic fields in transferring the power, it is comparatively safer than CPT which uses electric fields.

3) IPT can use broad frequency ranges from 10 kHz to 10 MHz, while CPT can use smaller range of frequencies from 100 kHz to 10 MHz.

There are other important advantages that play a main role behind using the IPT technique in this system:

1) **Environmentally Friendly**: IPT can work in harsh environments as it has two independently enclosed parts. It is not much affected by dirt, dust or chemicals. It does not produce any kind of carbon residues that might have harmful effects on surroundings. One concern that was raised in IPT is regarding the magnetic effect on human beings. However, some research carried out at the medical school of the University of Auckland shows that there are no observable negative biological effects at low frequency ranges [21]. These low frequencies usually do not have enough power density to heat the human body cells unlike the radio frequencies.

2) **Robustness and Reliability:** There is no electrical erosion or wear and tear in these systems as there is no direct friction. The electrical components of this system are closed completely; thus, it does not encourage any kind of chemical erosion in the conductor parts. Thus, there is less maintenance required.

Although many advantages were mentioned related to IPT, there are few limitations in IPT. The power levels of these systems are not suitable for industrial applications. IPT cannot afford strong coupling between the transmitter and receiver. Due to this loose coupling, it is next to impossible for them to be applied in high power applications. Also, misalignment in the placement of the coils might affect the IPT system performance. In [22] it is stated that when the coils are placed in 25% of misalignment, efficiency decreases to 92%. Due to these drawbacks, IPT alone cannot be used for designing EV systems. In order to overcome the drawbacks of IPT, this system adopts resonant systems into the IPT system, which can help IPT in increasing the system

performance. The features and advantages of implementation of these resonant circuits will be discussed in the following chapter.

1.5 Objective of this project

The aim of this thesis is to design, simulate and analyze a 5KW Resonant Inductive Wireless power transfer system for EVs to integrate them with MVDC networks, with advantages like improving system performance compared to conventional EV systems. The system designed in this thesis can fit commercial electric vehicle applications. Although there are many existing EV systems that are integrated with the AC grid, this project integrates EVs with MVDC systems.

To overcome the disadvantages of IPT, resonant circuits can be integrated into the WPT systems with IPT. In resonant circuit, the supply frequency is made equal to the circuit resonant frequency and when the system is at resonance, it shows high performance. This model system makes use of this advantage and aims at developing a system with improved performance. The main circuit is first tested in the simulation and then implemented in the hardware. The values of the components are calculated after deriving the equations for each component. These calculations are compared to the simulation and hardware results to verify the practicality of the designed model.

1.6 Thesis Outline

Chapter 1 introduces EVs, MVDC networks and their advantages, and integration of EVs with MVDC networks. It emphasizes using WPT in EVs and its advantages. It discusses existing WPT methods and examines how existing IPT methods in EVs can be improved in performance by using resonant systems in this thesis model.

Chapter 2 discusses resonant inductive power transfer and its features. It explains the design approach followed in this thesis for a 5KW WPT system. It elaborates on the block diagram and parts like the PWM Module containing the controller circuit and driver circuit and the role they play in the system's design. It also discusses the inverter power conversion stage and resonant circuits implemented in the design.

Chapter 3 describes the simulation design and analysis of the main circuit model. It shows the derivation and theoretical calculations of the main circuit components used in the model. The analysis and simulation results of the system are examined in detail.

Chapter 4 includes the hardware test results of the proposed system. It examines the comparison between the simulation and hardware test results. It reviews the output results for the experiment performed at different distances between the transmitter and receiver at different load conditions.

Chapter 5 concludes by explaining how the designed system can be verified for practical applications.

CHAPTER 2

RESONANT CIRCUITS OF INDUCTIVE WPT SYSTEM

2.1 Resonant Inductive power transfer

Early work on integrating WPT with resonance was started by Tesla, who explained the advantages of tuning the transmitting and receiving coils at resonance frequency, which is like the concept of an oscillation transformer. The oscillation transformer is the main principle behind the integration of resonance with WPT [23, 24]. As discussed in chapter 1, resonant circuits are implemented along with the IPT in order to increase the coupling and performance of the IPT system. Application of resonant circuits can increase the transmitting distance of the IPT systems. Resonant circuits are applied to get the resonance frequency, which can improve the rate of energy transfer. A resonator consists of a combination of an inductor and capacitor. This technique of combining inductive coupling and resonance is known as magnetic resonance coupling. Magnetic resonance coupling enables the interactions between two objects very strongly [25-28]. In this technology, energy can be transferred from the source to the receiver very efficiently, with very little loss of energy. It is highly efficient, with negligible radiation losses and provides great range and directionality when compared to the conventional IPT [29].

Because of the resonance property, magnetic resonance coupling is immune to the neighboring environment. In an IPT system without resonance, the power transfer between the transmitter and receiver can decrease if there is a misalignment in the positions of primary and secondary coils, but inclusion of resonant circuits can give flexibility in the orientation between the source and load during the operation [30, 31]. One of the most advantageous features of magnetic resonance coupling is that it can also be applied between one transmitter and many

receivers. It can transmit the power even if the multiple load devices have different power requirements. This technique is leading in the research field, and because of these advantages it is being applied in EVs [25], consumer electronics, biomedical implants, wireless sensor networks, and robotics power supplies.

In an electric circuit, electrical resonance is a phenomenon that occurs at a particular frequency known as resonant frequency when the imaginary parts of impedances or admittances of the elements of circuit cancel each other out. The response of a circuit is maximized at this particular resonant frequency. Resonance can occur in any circuit that has a combination of an inductor and a capacitor as both these elements can store the energy [32]. In a resonant circuit, the energy will be oscillating between both the inductor and capacitor and the rate of transfer of the energy between these two elements depends on the values of L and C. Because of these energy transfer oscillations, we will see oscillations in the circuit. If this circuit is ideal, and if there is no presence of any kind of resistive elements, these oscillations will continue forever. In reality, though, all the circuits will have some resistance involved in them. Because of the presence of this resistance, there will be depreciation in these oscillations. To maintain these oscillations, we must provide supply from an external source with the same frequency to this LC circuit (which was addressed as resonant frequency). This way we can maintain the oscillations. Parallel and series RLC circuits are the two main basic resonance circuits. In resonance circuits, the sharpness of the resonance can be measured by a term called Quality factor. The Quality factor is given by the formula below.

$$Q = 2\pi \times \frac{Maximum\ energy\ stored\ in\ the\ circuit}{Energy\ dissipated\ by\ the\ circuit\ in\ one\ period\ at\ resonance}$$

In a series resonant circuit, this Quality factor is given by equation below.

$$Q = \frac{\omega_o L}{R} = \frac{1}{\omega_O CR} = \frac{1}{R}\sqrt{\frac{L}{C}} \qquad .$$ (1)

Whereas in a parallel resonant circuit, it is given by following equation.

$$Q = \frac{R}{\omega_o L} = \omega_O RC = R\sqrt{\frac{C}{L}} \qquad .$$ (2)

By using these concepts of basic resonance circuits, the equations for the main circuit model used in this system model are derived, which will be discussed in the next chapter. Another main advantage of resonant circuits that makes them suitable for IPT applications is that they can boost the voltage and current levels depending on their topology. For example, a series resonant circuit can act as a voltage amplifier and a parallel resonant circuit can act as a current amplifier. When the circuit applied acts as a voltage amplifier, the voltage produced at the resonant circuit will be very high compared to the input supply voltage.

In a series circuit, at Resonance, the voltage across the inductor can be given by equation 3.

$$V_L = \frac{V_m}{R}\omega_o L$$ (3)

We know that, $\frac{\omega_o L}{R}$ is the Quality factor Q, so in the above equation, if we replace that term with Q, we get equation 4.

$$V_L = V_m Q \qquad .$$ (4)

From the above equation, it is evident that the voltage across the inductor will be much larger than the input supply voltage; hence, this circuit can act as a voltage amplifier. The same concept can

be applied for the voltage across the capacitor, so by properly designing the values of L and C in the resonant circuit, we can acquire higher voltages at higher frequencies.

2.2 5 KW IPT system design approach:

The block diagram of the system design used in this model is shown in Fig 3. Any wireless power transfer system has two main parts, the transmitter and the receiver. It needs an input power which can be given from either an AC or a DC source.
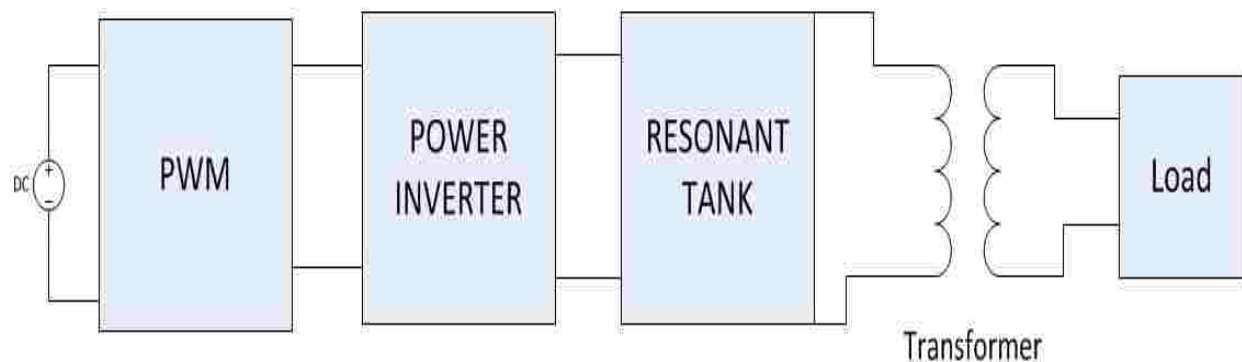
Fig 3. 5KW system design approach

In this work, as shown in Fig 3, on the transmitter side, power electronics converters are used which transform DC supply to AC with desired frequency. A full bridge inverter topology is being used for this purpose. As stated in chapter 1, in many WPT models, a two-stage AC-DC-AC conversion process was used, but this whole process needs circuitry involving switching devices. The more switching devices there are, the more switching losses there are. To overcome this, in [33] a few AC-AC one stage conversion models were discussed, but it is also stated that one stage

AC-AC converters with resonant circuits might not be suitable due to the difficulty in control and unstable outputs in these converters, so in this model integrating the system with MVDC has an advantage of one stage DC-AC conversion. In general, in wireless charging systems for EVs, the resonant frequency or the switching frequency of an inverter ranges from 20 KHz to 100 KHz.

In this model, MOSFETs are used for switching purposes in the inverter. In general, MOSFETs have two kinds of losses, known as conduction and switching losses [35, 36]. The switching losses occur while turning the switch ON and OFF. The switching losses involved in these switches during ON and OFF are given by the formulae below.

$$\text{Turn ON power losses: } P_{on} = E_{on}f_{sw} \tag{5}$$

$$\text{Turn OFF power losses: } P_{off} = E_{off}f_{sw} \tag{6}$$

where,

E_{on} and E_{off} are energies dissipated at the switch during ON and OFF, and f_{sw} is the switching frequency.

From the above two formulae, it is evident that the switching losses are directly proportional to the switching frequency. Choosing higher frequencies can make the system more compact, but as shown above, increase in frequency can lead to switching losses. Also, the EMF emissions which can be introduced by the high frequencies should also be studied. Decreasing the power conversion stages will reduce the switching losses.

2.2.1 PWM Module:

The system consists of a PWM module, which consists of two circuits that generate pulses to control the switches in the inverter. These two circuits are:

1) Controller IC

2) Driver circuit.

The controller controls the inverter switches by phase shifting the switching of one half bridge with respect to the other, allowing constant frequency pulse width modulation. It provides the signals to the driver circuit, which is an interface between the controller and the switches.

2.2.2 Purpose of gate driver circuit

In general, MOSFETs have some parasitic capacitance because of their structure. This parasitic capacitance can limit the switching speed of MOSFET. Usually, the input parasitic capacitance which is the total of gate source capacitance and gate drain capacitance when seen from the input, must be charged in order for the MOSFET to turn ON, so this parameter is important in practical applications. This parasitic capacitance at the input must be charged at least to the minimum gate voltage required for the MOSFET to operate. To turn OFF the transistor, this capacitance should be discharged.

Also, when the MOSFET is switched on or off, it might not start conducting immediately and might conduct high current. The gate current that is applied to MOSFET to turn it ON, can produce a certain amount of heat which might even damage the MOSFET in a few cases, so in order to decrease the switching losses, decreasing the switching time might be necessary, but the decrease in switching time might requires more current to charge the gate. The control signal that

is generated from the microcontroller is limited to current whose magnitude is in the range of a few milli amperes.

With this small amount of current, the MOSFET will turn ON very slowly producing considerable switching losses. Also, the parasitic capacitance mentioned before might draw current very fast, which might lead to excess current draw causing damage to the hardware involved. The usage of gate drivers might prevent all this damage from happening. The gate driver can produce a high current input for the MOSFET gate. This can reduce the switching time and the switching losses. In this way, the gate driver prevents the switches from damage and acts as an interface between the controller and power switches.

2.3 Main circuit of 5KW system

The main circuit diagram of this system model is shown in Fig 4. In the main circuit diagram, we can see two main parts on the transmitting side:

1) Inverter circuit
2) Resonant circuit.
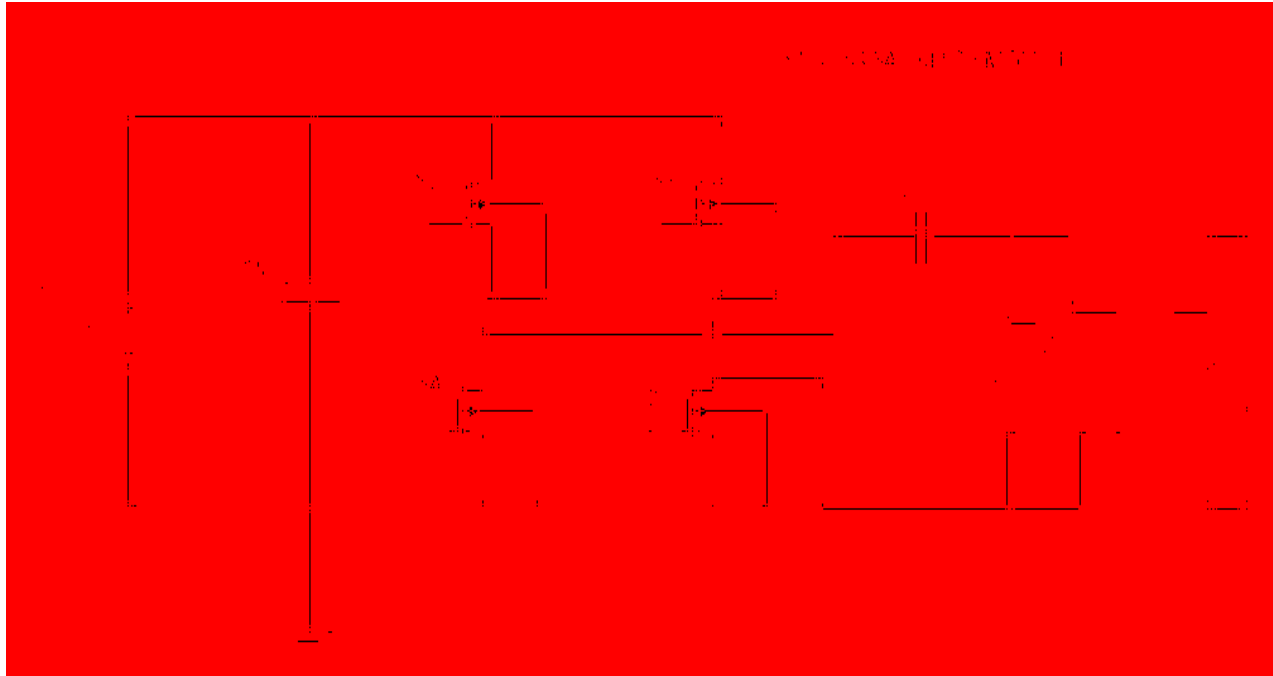
Fig 4: Main circuit diagram of the 5KW proposed model

2.3.1 Inverter of 5KW main circuit:

The inverter of the proposed main circuit converts the DC supply to AC and feeds it to the resonant circuit. In general, there are many inverter resonant circuit topologies currently being used in practical WPT applications. In [33], a few resonant inverter topologies are explained and a few are listed below.

1) Class E resonant inverter

2) Class D resonant inverter

3) Class DE resonant inverter

Even though there are many more topologies, in [33] it is stated that the class D and full bridge class D resonant inverters are most popular in practical applications of WPT due to easy system

parameter design. The full bridge class D type is a H bridge inverter connected to the resonant circuit. The same topology is used for the inverter design in this system model. The peak-peak voltage across the switch in full bridge Class D is twice as high as the DC supply voltage. Thus, this topology can produce a higher voltage to feed the LC resonant circuit, compared to the Class D half bridge type, making it more suitable for low DC supply applications. The switching frequency for this system is chosen to be 50kHz.

In the two half bridges in this inverter circuit, only one of them will be ON at a time. The switches are run complementary to get the desired output. There are four total combinations that are valid for a full bridge inverter. If the input voltage being supplied is referred to as Vin, the different stages of the full bridge inverter are shown in table 1.

Table 1: Different stages of full bridge inverter.

S1	S2	S3	S4	Vo (Inverter output voltage)
ON	ON	OFF	OFF	Vin
ON	OFF	ON	OFF	Zero
OFF	OFF	ON	ON	-Vin
OFF	ON	OFF	ON	Zero

From the above table, one can understand the output of the inverter according to the different switching actions of the switches.

2.3.2 Resonant circuit

From Fig 4, the capacitor and inductor named Cr and Lr are resonant capacitor and resonant inductor, respectively. As stated before, these two components play a major role in the circuit design, as they are crucial in creating the resonance condition and improving the performance of the IPT system. The values of these components are calculated using a few equations that are derived and discussed in the following chapter.

This system model uses the full bridge inverter design due to its simple and easy to implement topology compared to the other inverter topologies and its ability to produce higher voltages at the output. Also, the inductive coupling despite the limited transmission range, the charging power can be high when the transmission distance is less than the coil diameter. However, resonant systems are used to improve the transferring ability and the usage of magnetic resonant systems are proved to increase the inductive power transfer systems' performance by attaining 90% efficiency when the transmitting distance is up to a meter [34]. Using these different modules with the stated advantages can increase the performance of this system model.

CHAPTER 3

CALCULATIONS AND SIMULATION RESULTS

3.1 Derivation of Equations

A few equations are derived to calculate the theoretical values of the main circuit. In the main circuit diagram, there is a load R_l on the secondary side of the transformer.

To simply the calculation, the transformer can be eliminated by referring the load resistor onto the primary side as shown in Fig 5. The resistor that is referred to the primary side is addressed as R_l'.
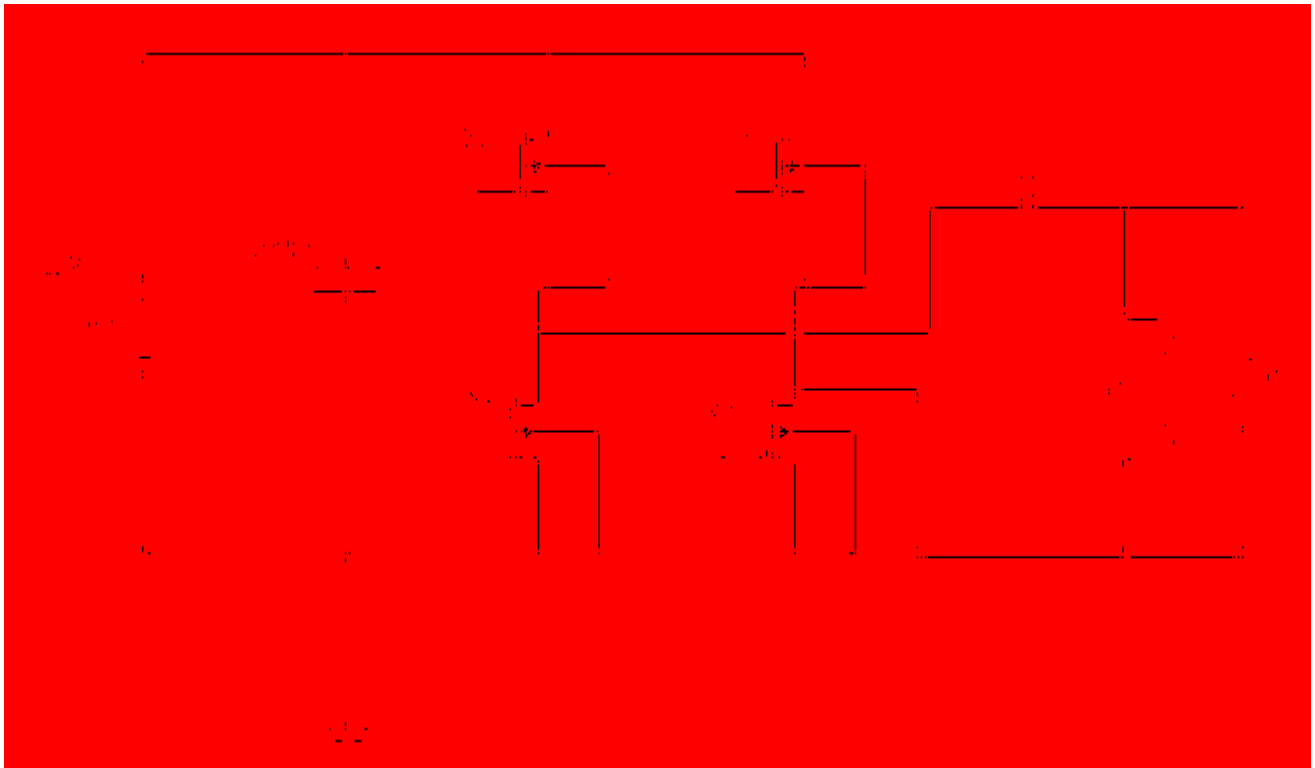
Fig 5: Main circuit with load resistor referred to the primary side

By following the basic concepts of a resonant circuit, the equations of the main circuit can be derived as shown below.

We know that in a circuit, at resonance condition, the imaginary components of the complex impedance or admittance are zero, so by calculating the total impedance of the circuit and equating the imaginary part to zero, we can solve for the circuit parameters at the resonance condition.

As shown in Fig 5, inductor Lr and the resistor R'_l are parallel to each other. Total Impedance Z is calculated by adding the impedance of Cr and impedance of parallel combination of Lr and R'_l.

Thus, the impedance of the parallel combination of Lr and R'_l is given by following equation.

$$Z_{L-R'} = \frac{R'\,(j\omega L)}{R' + j\omega L}$$

Total Impedance is given by equation below.

$$Z = \frac{1}{j\omega C} + \frac{R'\,(j\omega L)}{R' + j\omega L}$$

$$Z = \frac{1}{j\omega C} + \frac{R'\,(j\omega L)}{R' + j\omega L}\,\frac{(R' - j\omega L)}{((R' - j\omega L)}$$

By simplifying the above equation, we get the following equation.

$$Z = \frac{1}{j\omega C} + \frac{(R')^2\,(j\omega L) + R'(\omega L)^2}{(R')^2 + (\omega L)^2}$$

Now, by separating the real part and the imaginary part, we get the equation below.

$$Z = \frac{-j}{\omega C} + \frac{(j\omega L)(R')^2}{(R')^2 + (\omega L)^2} + \frac{(\omega L)^2\,R'}{(R')^2 + (\omega L)^2}$$

$$Z = \frac{(\omega L)^2 R'}{(R')^2 + (\omega L)^2} + \frac{(j\omega L)(R')^2}{(R')^2 + (\omega L)^2} - \frac{j}{\omega C}$$

$$Z = \frac{(\omega L)^2 R'}{(R')^2 + (\omega L)^2} + j\left(\frac{(\omega L)(R')^2}{(R')^2 + (\omega L)^2} - \frac{1}{\omega C}\right)$$

From the above equation, if we equate the imaginary component to zero, we get the following

equation.

$$\left(\frac{(\omega L)(R')^2}{(R')^2 + (\omega L)^2} - \frac{1}{\omega C}\right) = 0$$

From the above equation the resonant frequency is obtained as follows:

$$\frac{(\omega L)(R')^2}{(R')^2 + (\omega L)^2} = \frac{1}{\omega C}$$

$$\omega^2 LC(R')^2 = (R')^2 + (\omega L)^2$$

$$\omega^2 LC(R')^2 - (\omega L)^2 = (R')^2$$

$$\omega^2(LC(R')^2 - L^2) = (R')^2$$

$$\omega^2 = \frac{(R')^2}{LC(R')^2 - L^2}$$

$$\omega^2 = \frac{1}{LC - \dfrac{L^2}{(R')^2}}$$

From the above equation, we can solve for ω and get the equation as below.

$$\omega = \frac{1}{\sqrt{LC - \frac{L^2}{(R')^2}}} \qquad (7)$$

From the above equation, by solving for capacitance, we get the final equation as shown below.

$$C = \frac{1}{L\omega^2} + \frac{L}{(R')^2} \tag{8}$$

From the above equation, we can find the value of capacitance by plugging in all the values of the variables in the equation. If the input voltage is given by V_{in}, at resonance the relation between voltage and current is given by the equation below.

$$V_{in} = I \left[\frac{(\omega L)^2 R'}{(R')^2 + (\omega L)^2}\right] \tag{9}$$

Thus, at resonance, the voltage drop in the resonant circuit will be only due to the real part of the total circuit impedance.

3.1.1 Input current

From equation 7, the equation for the input current at resonance will be,

$$I = V_{in} \left[\frac{(R')^2 + (\omega L)^2}{(\omega L)^2 R'}\right] \tag{10}$$

3.1.2 Quality Factor

The quality factor for this circuit can be found by transforming the circuit into an equivalent series RLC circuit as shown in Fig 6.
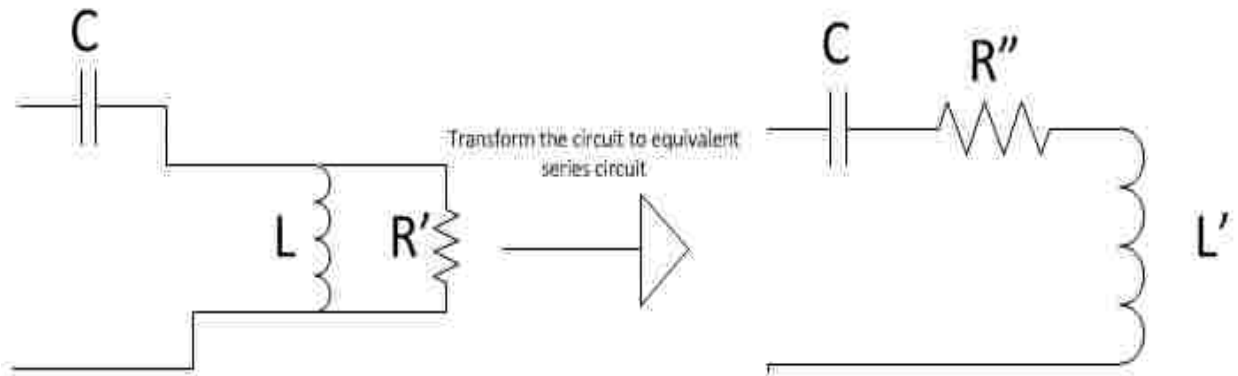
Fig 6: Transforming to equivalent series RLC circuit

Now by transforming the main circuit into the form of a series RLC circuit, the Quality factor can be derived as follows.

From Fig 6,

$$\frac{1}{\frac{1}{j\omega L} + \frac{1}{R'}} = j\omega L' + R''$$

Now, to simplify, the numerator and denominator are multiplied by $R' - j\omega L$

$$\frac{j\omega LR'}{j\omega L + R'} \times \frac{R' - j\omega L}{R' - j\omega L} = j\omega L' + R''$$

$$\frac{j\omega LR'(R' - j\omega L)}{(R')^2 + (\omega L)^2} = j\omega L' + R''$$

$$\frac{j\omega L(R')^2}{(R')^2 + (\omega L)^2} + \frac{(\omega L)^2 R'}{(R')^2 + (\omega L)^2} = j\omega L' + R''$$

By comparing LHS and RHS, we get,

$$R'' = \frac{(\omega L)^2 R'}{(R')^2 + (\omega L)^2} \tag{11}$$

$$L' = \frac{L(R')^2}{(R')^2 + (\omega L)^2} \tag{12}$$

For a series RLC circuit, the quality factor is given by,

$$Q = \frac{\omega L'}{R''}$$

By substituting L' and R'' in the above equation, we get,

$$Q = \omega \frac{L(R')^2}{(R')^2 + (\omega L)^2} \times \frac{(R')^2 + (\omega L)^2}{(\omega L)^2 R'}$$

By solving the above equation, we get the equation for the quality factor as,

$$Q = \frac{R'}{\omega L} \tag{13}$$

The above equation of Quality factor is in terms of inductance. Another equation can also be

derived which is in terms of the Quality factor and capacitance. For series RLC circuit, the

Quality factor in terms of capacitance is given by,

$$Q = \frac{1}{\omega C R''}$$

In the above equation, by substituting R'' we get,

$$Q = \frac{1}{\omega C\left(\frac{\omega^2 L^2 R'}{(R')^2 + \omega^2 L^2}\right)}$$

$$Q = \frac{(R')^2 + \omega^2 L^2}{\omega C\,[\omega^2 L^2 R']}$$

$$Q = \frac{\frac{(R')^2}{\omega^2 L^2} + 1}{\omega C R'}$$

$$Q = \frac{Q^2 + 1}{\omega C R'}$$

$$\frac{Q}{Q^2 + 1} = \frac{1}{\omega C R'} \qquad (14)$$

Both equations 6 and 12 can be solved to find the value of Capacitance.

3.1.3 Voltage across Capacitor

The voltage across the capacitance can be calculated as shown below.

The voltage across capacitor can be given by,

$$V_C = I X_C$$

$$V_C = V_{in}(\frac{(R')^2 + (\omega L)^2}{(\omega L)^2 R'}) \, (\frac{1}{\omega C})$$

From the above equation, the magnitude of the Voltage across the capacitor is given by,

$$V_C = V_{in}(\frac{(R')^2 + (\omega L)^2}{(\omega L)^2 R'}) \, (\frac{1}{\omega})(\frac{L\omega^2 (R')^2}{(R')^2 + L^2 \omega^2})$$

$$V_C = V_{in} \left(\frac{L\omega (R')^2}{(\omega L)^2 R'} \right)$$

$$|V_C| = V_{in}(\frac{R'}{\omega L})$$

In the above equation, the term $\frac{R'}{\omega L}$ is nothing but the Quality factor Q.

If we replace that term with Q, we get the equation for voltage across the capacitor as,

$$|V_C| = V_{in}Q \tag{15}$$

3.1.4 Voltage across Inductor

The voltage across the inductor can be calculated as shown below.

Here, in the main circuit when the secondary side resistor is referred on to the primary side, inductor and resistor are in parallel.

Fig 7. shows the phasor diagram for the parallel combination of inductor and resistor. From this Fig 7. the total current through the circuit can be calculated by the resultant of the vectors of inductor current and resistor current.
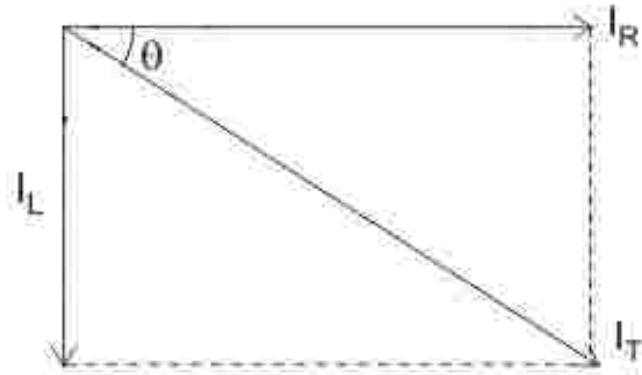
Fig7: Phasor diagram for parallel LR circuit

From equation 8, we know that at resonance the total current is given by,

$$I = V_{in}\left[\frac{(R')^2+(\omega L)^2}{(\omega L)^2 R'}\right]$$

The total current obtained from the resultant of the two vectors is equal to the above current equation, so

$$\sqrt{(I_{R\prime})^2 + (I_L)^2} = V_{in}\left[\frac{(R\prime)^2 + (\omega L)^2}{(\omega L)^2 R\prime}\right]$$

$$\sqrt{\left(\frac{V_L}{R\prime}\right)^2 + \left(\frac{V_L}{X_L}\right)^2} = V_{in}\frac{(R\prime)^2 + (\omega L)^2}{(\omega L)^2 R\prime}$$

$$V_L\sqrt{\left(\frac{1}{R\prime}\right)^2 + \left(\frac{1}{\omega L}\right)^2} = V_{in}\frac{(R\prime)^2 + (\omega L)^2}{(\omega L)^2 R\prime}$$

$$R\prime V_L\sqrt{\left(\frac{1}{R\prime}\right)^2 + \left(\frac{1}{\omega L}\right)^2} = V_{in}\frac{(R\prime)^2 + (\omega L)^2}{(\omega L)^2}$$

By replacing $\frac{R\prime}{\omega L}$ by Q, we get,

$$V_L\sqrt{1 + Q^2} = V_{in}(Q^2 + 1)$$

$$|V_L| = V_{in}\sqrt{1 + Q^2} \tag{16}$$

3.1.5 Inductor Current

The current through the inductor can be calculated by

$$I_L = \frac{V_L}{L \times \omega} \tag{17}$$

The current through the capacitor will be the same as the total current of the circuit.

3.2 Theoretical Calculations for 5KW circuit

The calculations of the circuit are done using the equations derived in the previous section. The specifications for the 5KW system are shown in table 2.

Table 2: Specifications of 5KW system.

Parameter	Value
Input Voltage	120 V
Power Rating	5KW
Operating Frequency	50kHz
Quality Factor	5
Output voltage	400 V
Turns ratio	2.5

Voltage across the Capacitor

The voltage across the capacitor is given by,

$$|V_C| = V_{in}Q$$

By substituting $V_{in} = 120V$ and Q = 5, we get,

$$|V_C| = 600 \text{ V (rms)} = 848.528 \text{ V(peak)}$$

Voltage across the Inductor

The voltage across the inductor is given by,

$$|V_L| = V_{in}\sqrt{1 + Q^2}$$

$$|V_L| = 120\sqrt{1 + 5^2}$$

$$|V_L| = 611.88 \text{ V (rms)} = 865.3323 \text{ V (peak)}$$

Value of Inductance

In the equation $= \frac{R'}{\omega L}$, $\omega = 2\pi f$ where f = 50KHz, as R' is the load resistor referred to the primary side, R' is given by,

$$R' = R\left(\frac{N_1}{N_2}\right)^2$$

In order to find the value of R', the value of R should be known.

The output voltage across the secondary terminals is calculated by,

$$\frac{V_L}{V_O} = \frac{N_1}{N_2}$$

where V_O is the output voltage across the secondary terminals and V_L is the voltage across the inductor.

By substituting the value of V_L = 611.88 V and $\frac{N_1}{N_2}$ = 2.5, V_O is obtained as,

$$V_O = 244.7529 \text{ V (rms)} = 346.1328 \text{ V (peak)}$$

As the output voltage is 244.7529 V and the power is 5KW, we can find the load resistor value by,

$$R = \frac{(V_O)^2}{P} = \frac{(244.7529)^2}{5000} = 11.98 \text{ } \Omega$$

By substituting the values of R and $\frac{N_1}{N_2}$, R' is obtained as,

$$R' = (11.98)(2.5)^2 = 74.875 \text{ } \Omega$$

Now the value of inductance can be found from the Quality factor.

We know that the Quality factor is given by,

$$Q = \frac{R'}{\omega L}$$

By bringing L on to the LHS we get,

$$L = \frac{R'}{\omega Q}$$

where $\omega = 2\pi f = 2\pi \times 50{,}000$

By substituting the value of $R' = 74.875\ \Omega$, $\omega = 2\pi \times 50{,}000$ and $Q = 5$, the value of L is obtained as,

$$L = \frac{74.875}{5 \times 2\pi \times 50{,}000} = 4.76669\ e\text{- }05\ \text{Henry}$$

Value of capacitance

The capacitance value can be found from the equation,

$$\frac{Q}{Q^2 + 1} = \frac{1}{\omega C R'}$$

$$\frac{C}{1} = \frac{Q^2 + 1}{\omega Q R'}$$

However, substituting all the values on the right hand side in the above equation, the value of capacitance is found to be,

$$C = \frac{26}{5 \times 2\pi \times 50{,}000 \times 74.875} = 2.2106\text{e-}07\ \text{Farad}$$

Total Input current

The total current through the circuit at resonance can be found from the formula,

$$I = V_{in}[\frac{(R')^2+(\omega L)^2}{(\omega L)^2 R'}]$$

$$I = V_{in}[\frac{Q}{\omega L} + \frac{1}{R'}]$$

$$I = \frac{5}{2\pi \times 50,000 \times 4.76669 \times 10^{-5}} + \frac{1}{74.875}$$

$$I = 41.669 \text{ Amperes}$$

Current through the Inductor

The current through the inductor can be found from the formula,

$$I_L = \frac{V_L}{L \times \omega}$$

$$I_L = \frac{611.88}{4.76669 \times 10^{-5} \times 2\pi \times 50,000}$$

$$I_L = 40.86 \text{ Amperes}$$

Current through the Capacitor

The current through the capacitor is equal to the input current through the circuit,

$$I_C = I = 41.669 \text{ Amperes}$$

The summarized table for the calculated values of the main circuit model is shown below.

Table 3: Calculated values of 5KW system.

Parameter	Value
Voltage across the Capacitor	600 V (rms) , 848.528 V(peak)
Voltage across the Inductor	611.88 V (rms) , 865.3323 V (peak)
Value of Inductance	0.0476669 mH
Value of Capacitance	0.22106 µF
Total Input Current	41.669 A(rms)
Current through the Inductor	40.86 A(rms)
Current through the Capacitor	41.669 A(rms)

3.3 The effect of frequency on the circuit parameters

The operating frequency or the resonance frequency value can vary the parameters of the circuit. As mentioned in the previous chapter, the increase in frequency can make the circuit more compact. However, too high frequency ranges can increase the losses in the system.

To check the frequency effect theoretically, the circuit parameters are calculated for three different frequencies, 20kHz, 30kHz and 50kHz. It is observed that for each frequency value, the values of Inductance and Capacitance have changed.

The values of L and C for different values of the mentioned frequencies are shown in table 4.

Table 4. L and C values for different frequencies

Frequency	Value of Inductance	Value of Capacitance
20kHz	0.11916 mH	0.552658 µF
30kHz	0.0794448 mH	0.368438 µF
50kHz	0.0476669 mH	0.22106 µF

The graphs below show the change in L and C values with respect to the operating frequency.

Fig 8: Frequency v/s Inductance
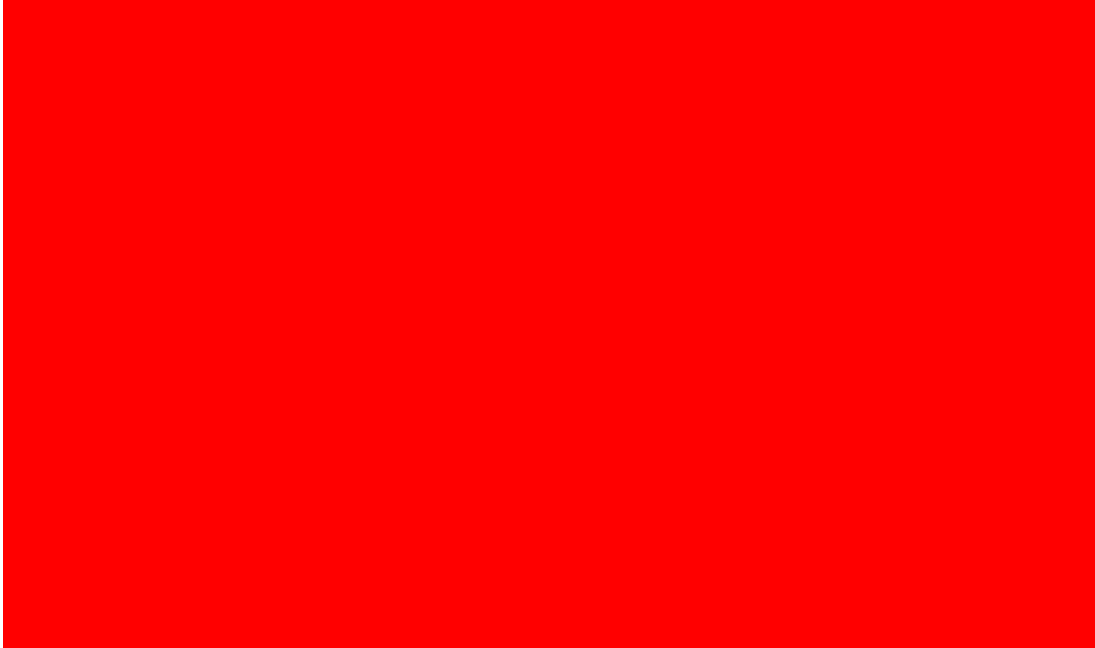
Fig 9: Frequency v/s Capacitance

From Fig 8 and Fig 9 it is evident that with the increase in frequency, there is a decrease in the values of L and C. This means that at higher frequencies the system can be designed with lower value components that make the system smaller. As the frequency decreases, the system becomes bulkier, so in this system, a higher frequency of 50kHz is used. Selecting higher frequencies can make the system compact, but the switching power losses and the effects of the magnetic fields should be taken care of.

3.4 Selection of the turns ratio for system design

The most suitable turns ratio should be selected and fixed to the system according to the system parameters. For this system, a turns ratio of 2.5 is selected due to the various observations made after analyzing the system parameters. The following analysis explains how fixing this turns the

ratio to 2.5. In this system, for turns ratio of 2.5, the output voltage obtained on the secondary side is 244.7529 V. Since the rated output voltage of the system is 400V DC, the voltage obtained on the secondary side can be converted to 400V DC, by using a DC-DC converter, after rectifying it. In order to reduce the power losses in the DC-DC stage, the value of the conversion ratio is maintained in the range [0.4,0.6].

A full wave rectifier can be used for the purpose of converting the AC voltage to DC, as the average DC output voltage of the full wave rectifier is higher when compared to the half wave rectifier. Firstly, in order to fix the turns ratio, the different outputs possible for the system should be determined. The system behavior is examined for four feasible different turns ratios, 1, 1.5 2 and 2.5. For the given specifications of the system, the possible output voltages for the system for different turns ratios are shown in the table below.

Table 5. Output voltages for different turns ratios

Turns Ratio	Output Voltage
1	611.8823 V (rms)
1.5	407.921 V (rms)
2	305.94117 V (rms)
2.5	244.7529 V (rms)

Case 1 (When turns ratio=1): For turns ratio =1, the output voltage obtained at the secondary side is 611.8823. For this case, as the output voltage on the secondary side is greater than 400 V, a buck converter can be used in the DC-DC stage. For a buck converter, the duty cycle is given by,

$$D = \frac{V_o}{V_i} \tag{18}$$

The voltage V_i is the input voltage to the DC-DC converter that is obtained from the rectifier output. The voltage V_o is the final output voltage at the DC-DC converter, which is 400V. If the conversion ratio is maintained between [0.4,0.6], the voltage input for the DC-DC converter should be in the range [400/0.6, 400/0.4], which is equal to [666.66V, 1000V]. To find the input voltage that is fed to the DC-DC converter, the average DC output voltage obtained from the rectifier should be calculated. For a full bridge rectifier, the equation for finding the value of the average DC output voltage is given by,

$$V_{dc} = \frac{2V_{max}}{\pi} = 0.637 \, V_{max} = 0.9 V_{rms}$$

where V_{rms} is the rms voltage of the ac input to the rectifier, so from the above formula the average DC voltage that will be obtained from the rectifier is obtained as,

$$V_{dc} = 0.9(\, 611.8823) = 550.69407 \, V$$

This voltage does not fall into the voltage conversion ratio range of DC-DC converter, so using turns ratio of 1 may lead to more losses in the system.

Case 2 (When turns ratio=1.5): For turns ratio = 1.5, the output voltage obtained at the secondary side is 407.92 V. At the output of the rectifier, the average DC voltage obtained will be,

$$V_{dc} = 0.9(407.92) = 376.128\ V$$

As this voltage is less than 400V, a boost converter can be used. For a boost converter, the duty cycle is given by,

$$D = 1 - \frac{V_i}{V_o} \tag{19}$$

If the conversion ratio is maintained between [0.4,0.6], the voltage input for the DC-DC boost converter should be in the range [240V, 160V] , but the average DC voltage obtained does not fall into this range, eliminating 1.5 as the turns ratio.

Case 3 (When turns ratio=2): For turns ratio = 2, the output voltage obtained at the secondary side is 305.94117 V. At the output of the rectifier, the average DC voltage obtained will be,

$$V_{dc} = 0.9(305.94117) = 275.247\ V$$

As in the previous case, the voltage does not fall into the DC-DC conversion ratio range, so this turns ratio would not be suitable for this system design.

Case 4 (When turns ratio=2.5): For turns ratio = 2.5, the output voltage obtained at the secondary side is 244.7529 V. At the output of the rectifier, the average DC voltage obtained will be,

$$V_{dc} = 0.9(244.7529) = 220.277\ V$$

In this case, it is evident that, the DC voltage falls into the desired range of [240V, 160V] of DC-DC stage, so compared to the previous compared cases, using the turns ratio of 2.5 would be a preferable option that can lead to fewer losses in the system. In this way, the most suitable output voltage on the secondary side and the turns ratio of the system are fixed. However, a few other constraints are examined to complete the system analysis in the following sections of this chapter.

3.5 System Parameter analysis for different turns ratios

For four different turns ratios mentioned in the previous section, the variations in the other system parameters like Quality factor, Voltages and Currents of Inductor and Capacitor, Inductance and Capacitance values are examined for the output voltage of 244.7529 V on the secondary side.

Variation of Quality factor:

The Quality factor is observed to be varying by change in the turns ratio of the system. When the turns ratio is decreased, it is observed that there is a decrease in the Quality factor.

The quality factors obtained for different turns ratios, are shown in the table below.

Table 6. Quality factors for different turns ratios

Turns ratio	Quality factor
1	1.777
1.5	2.891
2	3.954
2.5	5

As the Quality factor decreases, the performance of the system decreases. Good Quality factors can increase the system performance by allowing improvement in the power transfer distance. However, for near field WPT methods, usually Quality factors are selected below 10. In

[37], it is stated that the quality factor is selected low because for high values of quality factors, the transferred power attenuates. Based on the industry standards, this system is designed at the Quality factor of 5.

Fig 10 shows the variation of the Quality factor with respect to the turns ratios. As shown in Fig 10, for turns ratio less than 2.5, the Quality factor of the system decreased, which is not desirable, so the turns ratio of this system is maintained at 2.5
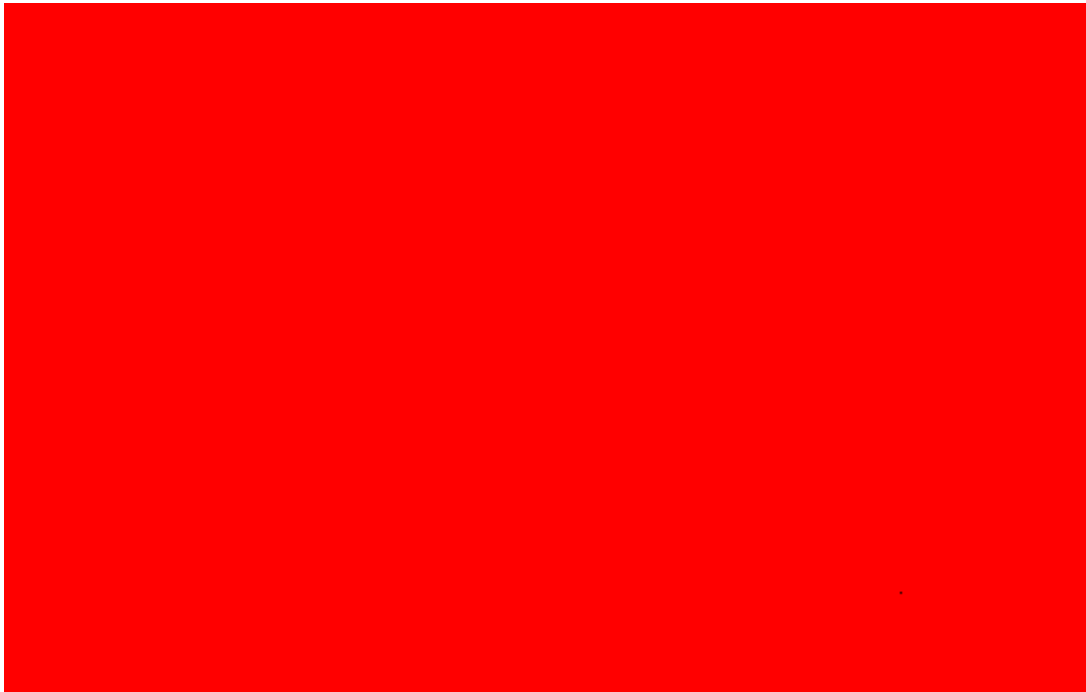

Fig 10: Variation of Quality factor with turns ratio

Variation of Inductance and Capacitance:

The change in the values of L and C are examined with the change in turns ratio. Table 7 and table 8 show the L and C values respectively, for different turns ratios.

Table 7. Inductance for different turns ratios

Turns ratio	Inductance
1	2.146e-05 H
1.5	2.9678e-05 H
2	3.8577e-05 H
2.5	4.76669e-05 H

Table 8. Capacitance for different turns ratios

Turns ratio	Capacitance
1	6.2167e-07 F
1.5	3.822e-07 F
2	2.7944e-07 F
2.5	2.2106e-07 F

Fig 11 and Fig 12 show the variation of Inductance and Capacitance for different values of turns ratios respectively.
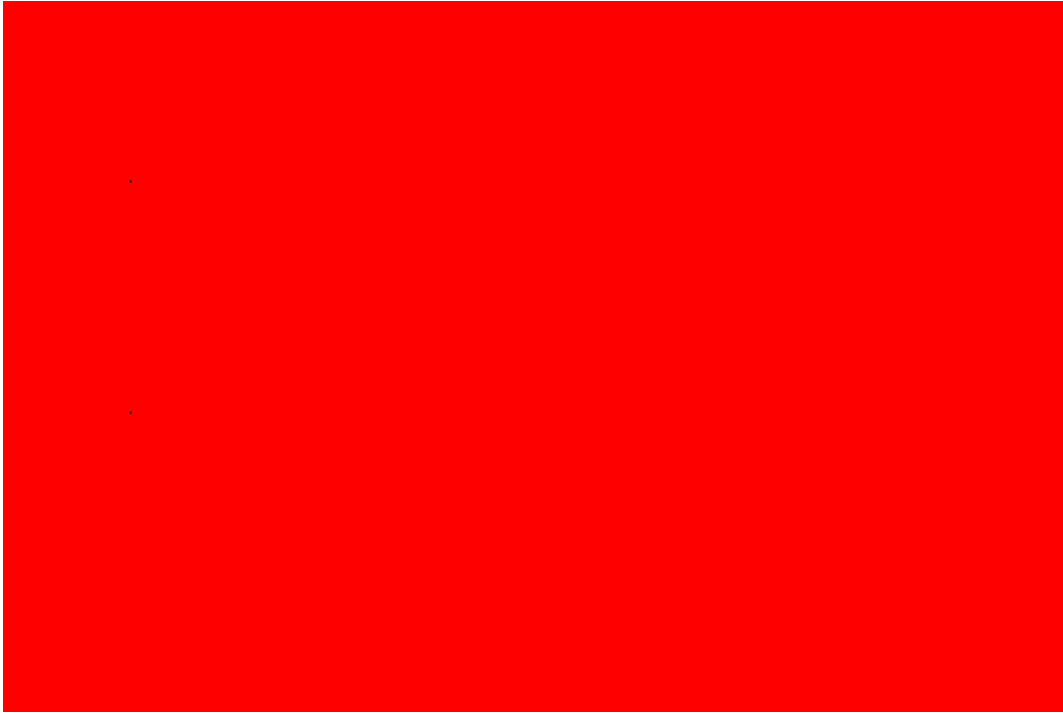

Fig 11: Variation of Inductance with turns ratio
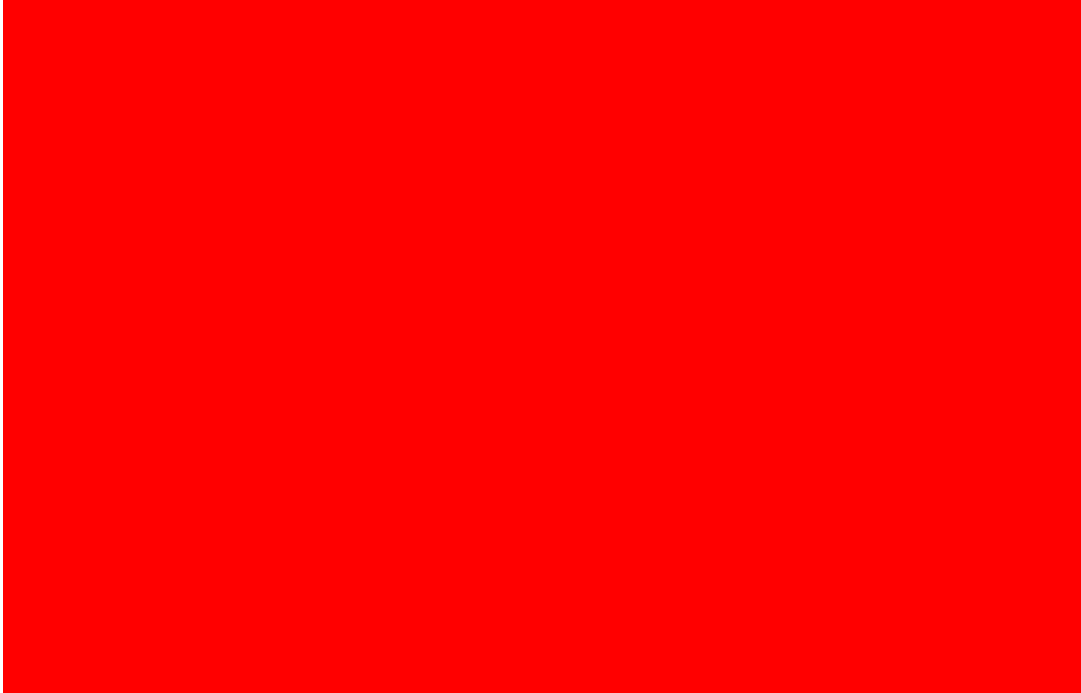
Fig 12: Variation of Capacitance with turns ratio

From Fig 11 and Fig 12 it is evident that even though there is a decrease in the inductance value with a decrease in the turns ratio, there is a considerable increase in the capacitance value. This increment can avoid the scope of decreasing the cost and weight of the system.

Variation of voltage across Inductor and Capacitor

The values of the voltages across the Inductor and Capacitor with respect to different turns ratios are shown in table 9 and table 10 respectively.

Table 9. Voltage across Inductor for different turns ratio

Turns Ratio	Voltage across the Inductor
1	244.686 V (rms)
1.5	367.0878 V (rms)
2	489.419 V (rms)
2.5	611.88 V (rms)

Table 10. Voltage across capacitor for different turns ratio

Turns Ratio	Voltage across the Capacitor
1	213.24 V (rms)
1.5	346.92 V (rms)
2	474.48 V (rms)
2.5	600 V (rms)

The variation of voltages across the inductor and capacitor can change the system capacity in transferring the power to the load. Fig 13 and Fig 14 show the variation of voltages across inductor and capacitor with turns ratios.

Fig 13. Variation of Inductor Voltage with turns ratio

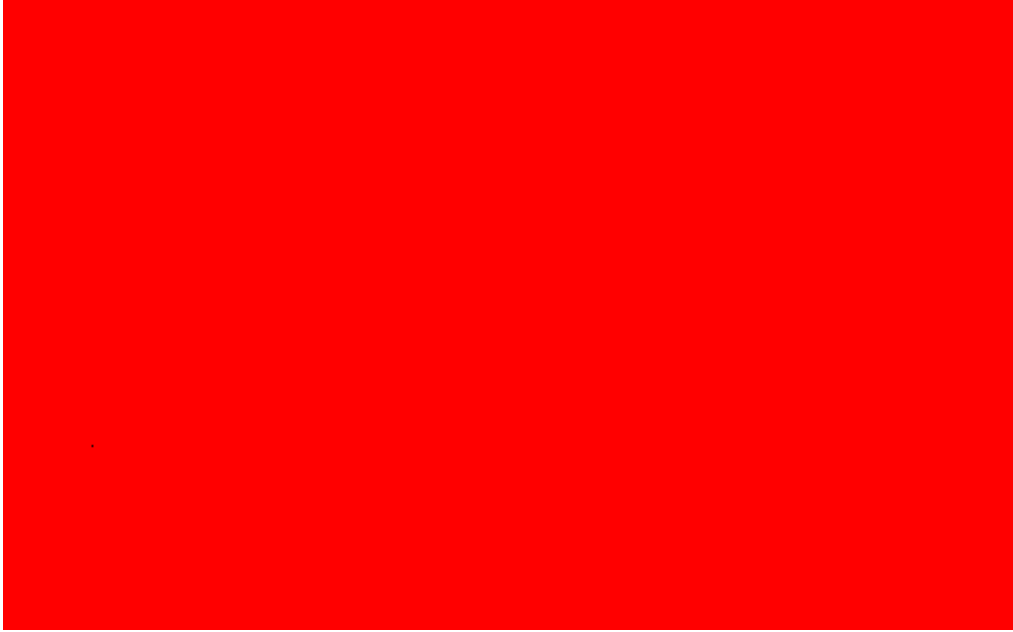Fig 14: Variation of Capacitor Voltage with turns ratio

At resonance, as the voltage drop in the circuit will be only across the resistive component, the sum of the voltages across the reactive components will cancel out. From tables 9 and 10 in this model it is evident that the magnitudes of voltage drop across Inductor and Capacitor are almost equal, and the voltages across these reactive components in the circuit altogether will become zero. As the turns ratio is reduced, the voltages across these elements are also reduced almost proportionally.

In this system, in order to transfer the energy from the primary side to the secondary side, the transformer takes the input from the resonant inductor, as it is connected across it, making the voltage across the inductor and primary windings equal. If the voltage across the inductor is decreased, for fixed output voltage, both the Quality factor of the circuit and the voltage across the primary windings are decreasing. With this, the ability of the system to transfer sufficient energy onto the secondary side decreases. This decrease in voltage also limits the range of distance between the primary and secondary coils to transfer the energy, which leads to poor system performance.

Variation of Current through Inductor

In this model, it is observed that as the turns ratio decreased, the value of current through the inductor decreased. Table 11 shows different magnitudes of current through the inductor for different turns ratios.

Table 11. Currents through the Inductor for different turns ratio

Turns ratio	Current through Inductor
1	36.294 A (rms)
1.5	39.3718 A (rms)
2	40.383 A (rms)
2.5	40.86 A (rms)

Fig 15 shows the variation of voltages across Inductor and capacitor with turns ratios.

Fig 15: Variation of Inductor Current with turns ratio

In Fig 15 we can see that as the turns ratio is decreased, the current through the inductor decreased. In this system model, the total input current through the circuit is divided between the inductor and the primary windings of the transformer. However, with the increase in the turns ratio, most of the current is flowing through the inductor. Compared to the current through the inductor, very little current flows through the primary windings. The total input current of the circuit will be the same irrespective of the turns ratio, so the decrease in the current through the inductor leads to an increase in the flow of the remaining current through the primary windings of the transformer.

From Fig 15, it is observed that there is considerable decrease in the current through inductor for every 0.5 decrease in the turns ratio. When the remaining current that flows through the primary winding of the transformer increases, the losses in the system increase. In a practical transformer, there are two types of losses, the core and the copper losses. The copper losses occur due to the power wasted in the form of I^2R loss due to the resistances of the transformer windings. The copper losses of these windings is given by,

$$P_{cu} = I^2R$$

From the above equation, it is evident that the copper losses are directly proportional to the square of current flowing through the windings, so the decrease in turns ratio might lead to an increase in the current flow through the transformer windings, leading to the increase in copper losses. In the case of the capacitor, as the current through the capacitor is equal to the input current, there will not be any change in capacitor current with the change in turns ratio.

The analysis done on all the system parameters with respect to the change in turns ratio show that at turns ratio = 2.5, the system performance is better compared to the other turns ratios.

3.6 Simulation Results for 5KW system

Fig 16 shows the simulation implementation of the main circuit design. The simulation is implemented in the MATLAB/SIMULINK platform. As shown in the simulation model, the gate signals for the inverter are given using a PWM generator. The output of the inverter feeds the resonant circuit, and the energy transfer from primary side to the secondary side takes place through the transformer, whose primary windings are connected across the resonant inductor. The calculations performed in the previous sections are implemented to the circuit in the simulation, and the outputs obtained are verified with the theoretical calculations.
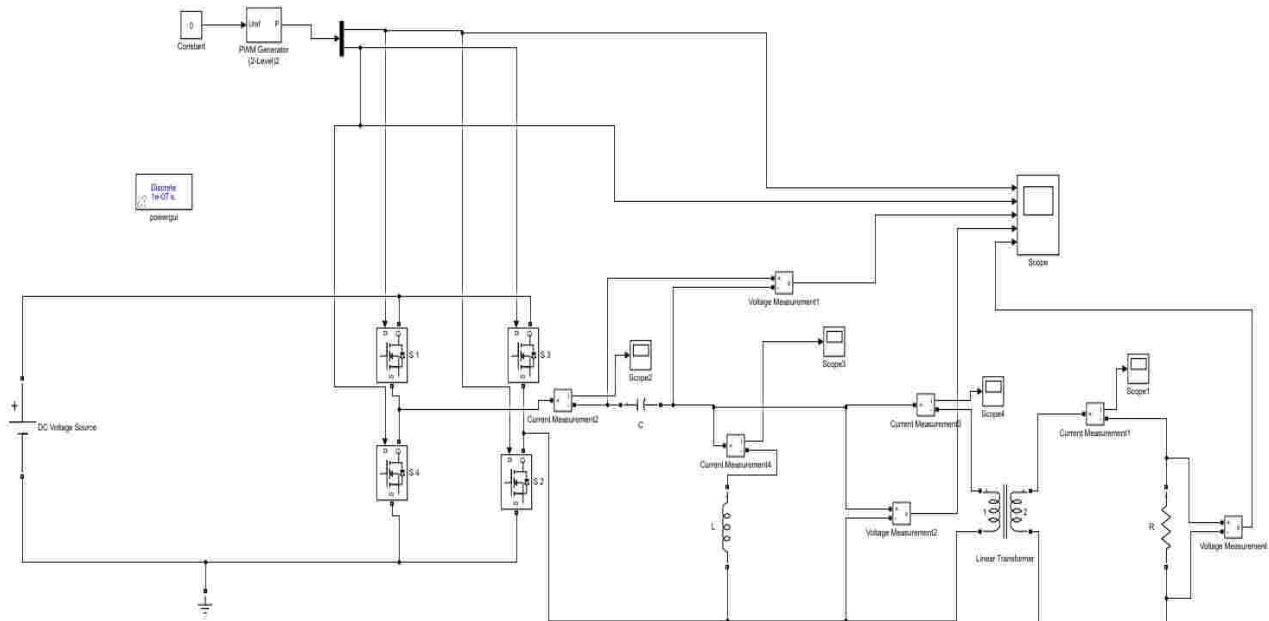

Fig 16: Simulation model of the 5KW main circuit

Fig 17 shows the whole image of the simulation system implementation of 5KW circuit.
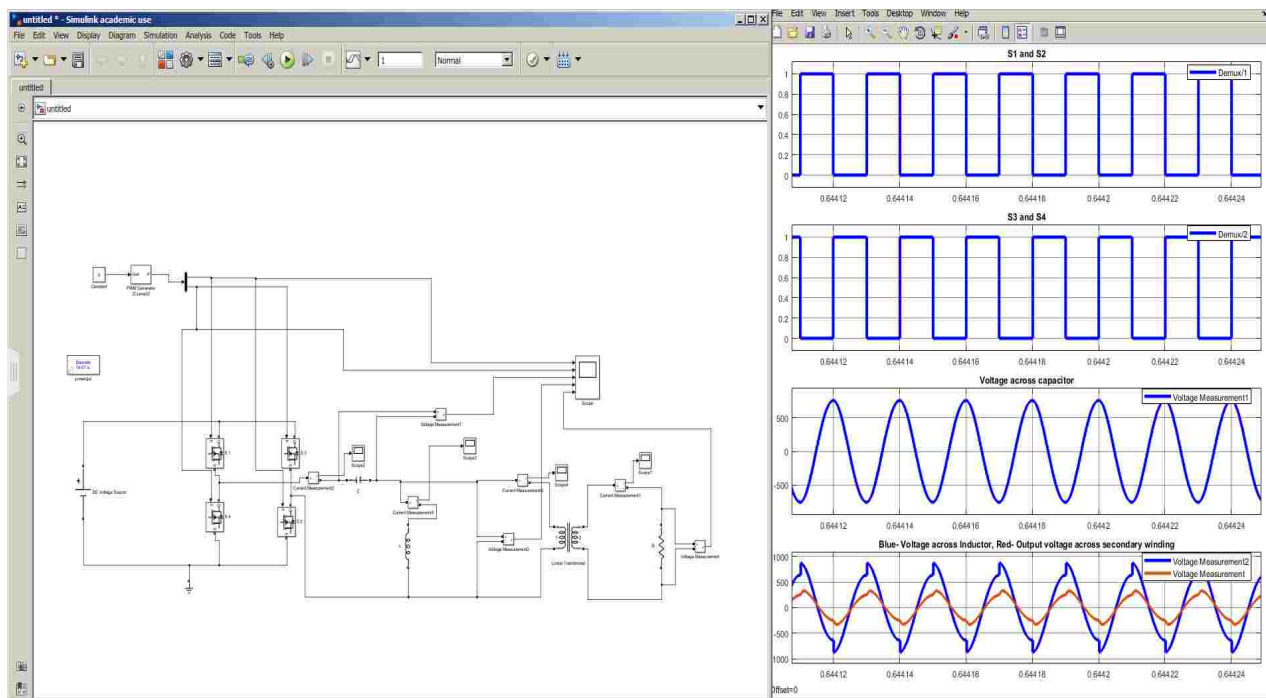
Fig 17: Simulation system of 5KW circuit

The output waveforms obtained in the simulation model are shown below in the following figures.

Output of inverter

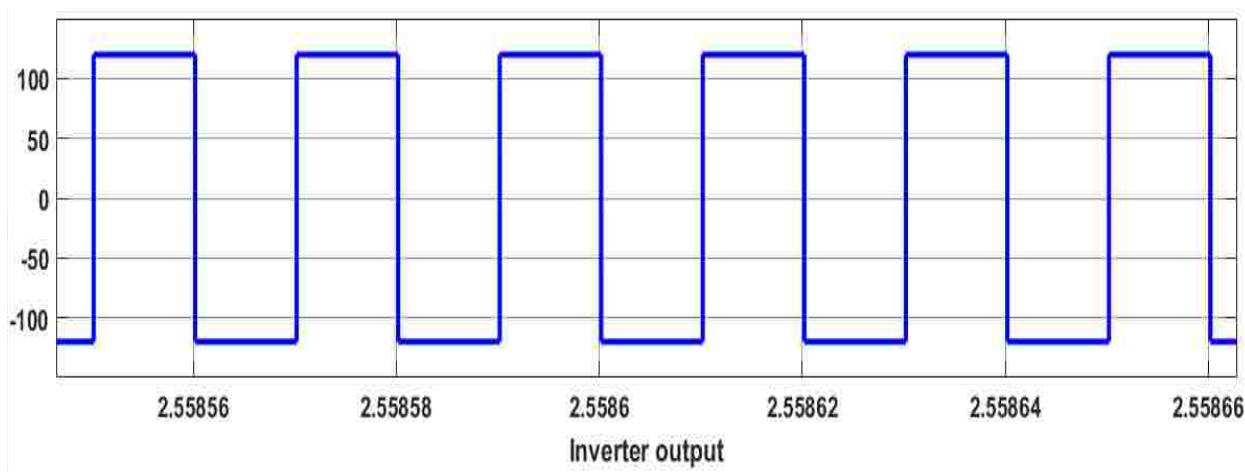Fig 18: Full bridge Inverter Simulation result of 5KW circuit

From Fig 18, it is evident that the 120V DC input voltage is changed to 120V AC voltage by the full bridge inverter.

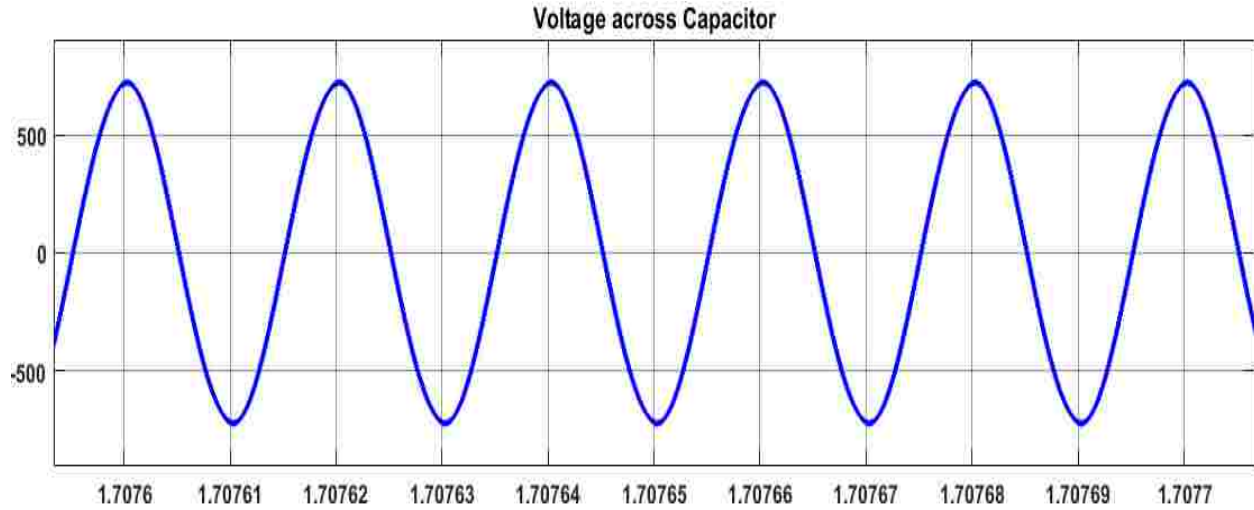**Output of voltage across capacitor**

Fig 19: Simulation result of voltage across Capacitor for 5KW circuit

Output of Voltage across Inductor
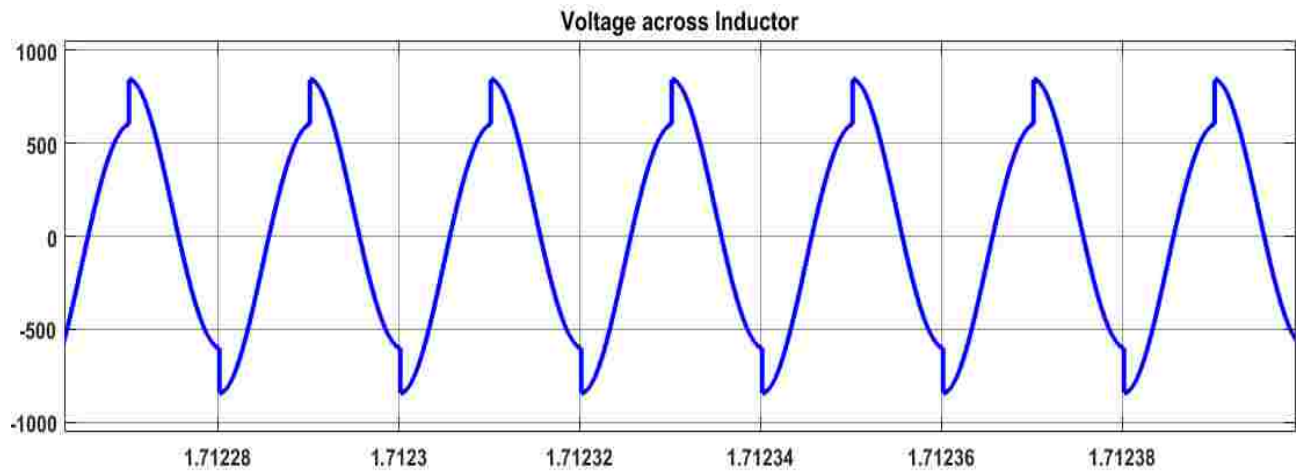
Fig 20: Simulation result of voltage across inductor for 5KW circuit

Input current
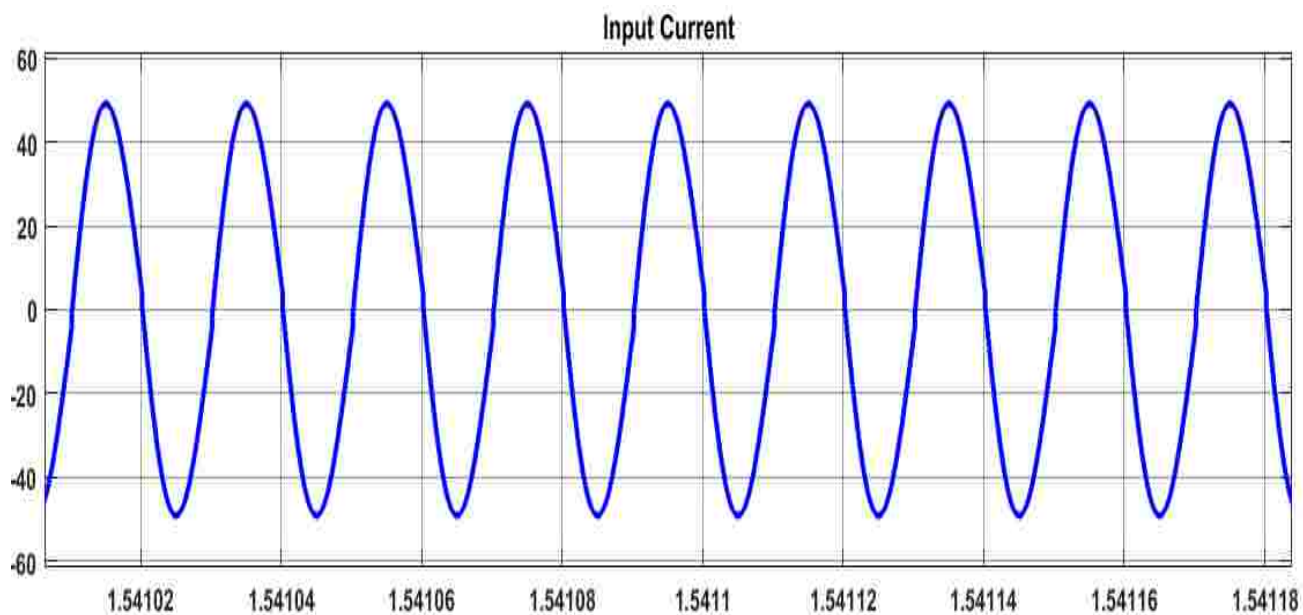
Fig 21: Simulation result of Input Current for 5KW circuit

Current through Inductor
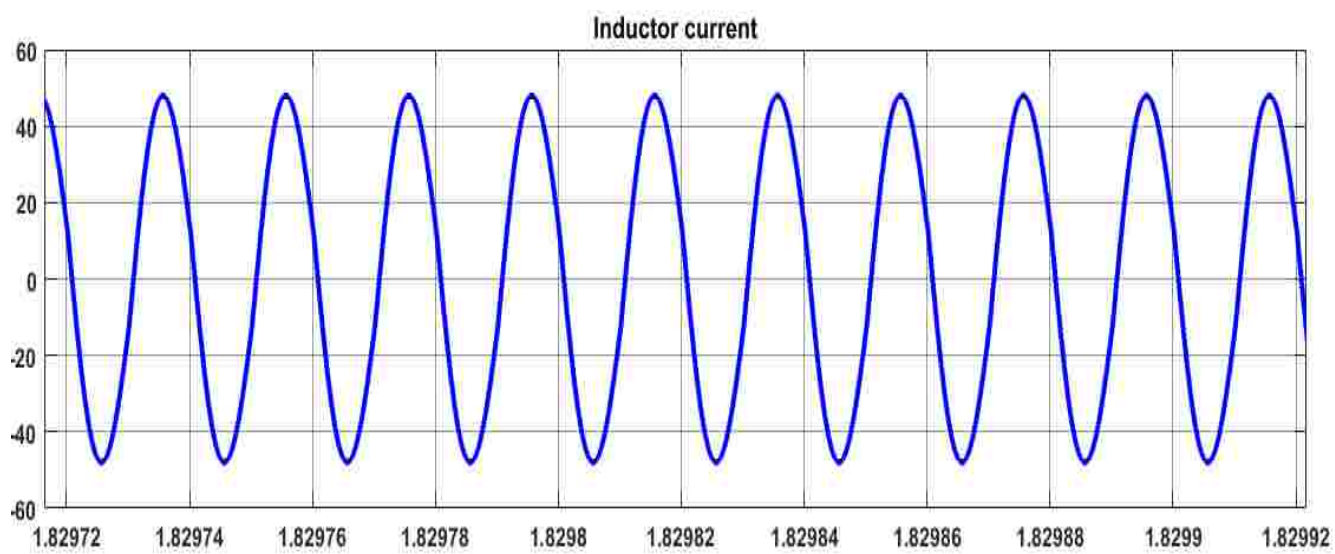
Fig 22: Simulation result of Inductor Current for 5KW circuit

Output Voltage across secondary winding

Fig 23: Simulation result of output Voltage across secondary winding for 5KW circuit

In the simulation results, it is observed that, the values from simulation are close enough to verify the theoretical calculations. Table 12 shows the comparison of the calculated values and the values obtained from the simulation.

Table 12: Comparison of theoretically calculated values and Simulation results

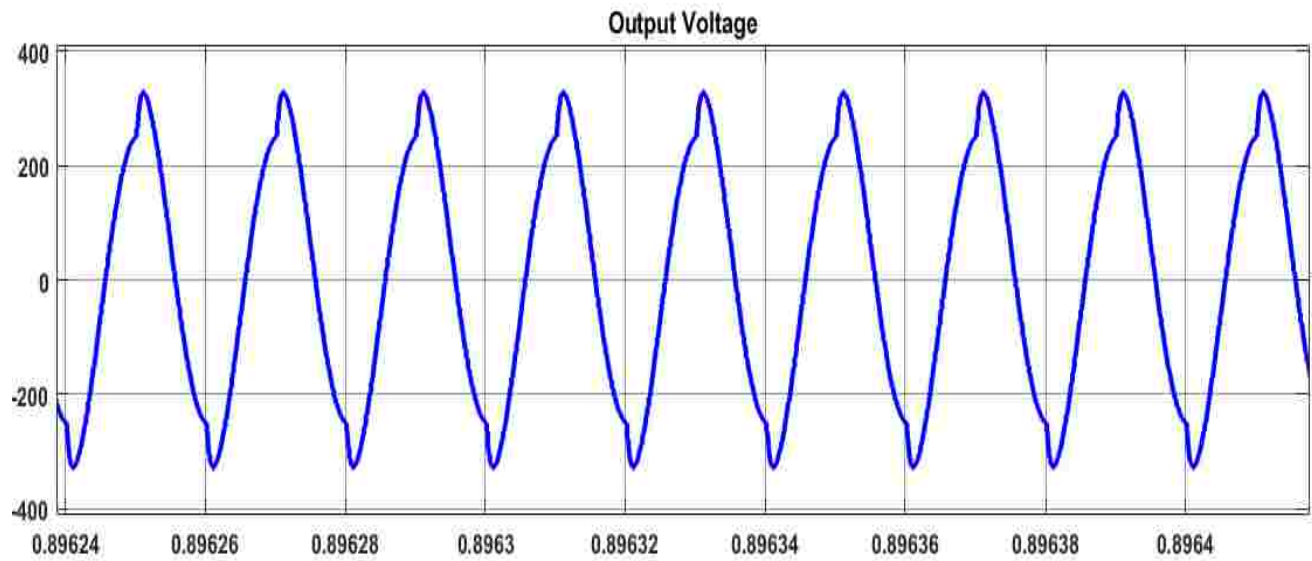| Parameter	Theoretically Calculated Value	Value obtained from the simulation
Voltage across Inductor	611.88 V (rms) 865.3323 V (peak)	867.5 V (peak)
Voltage across Capacitor	600 V (rms) 848.528 V (peak)	770.5 V (peak)
Input Current	41.669 A (rms) 58.928 A (peak)	52.25 A (peak)
Current through Inductor	40.86 A (rms) 57.78 A (peak)	49.95 A (peak)
Output Voltage on the secondary side	244.75 V (rms) 346.13 V (peak)	327 V (peak)

The same turns ratio of 2.5 is considered for this simulation model to verify the analysis done in this chapter previously. From the above table, it is evident that the calculated values are close to the simulation results for all the system parameters. Hence, from the simulation results, it is proved that the system design is verified by the simulation for 2.5 turns ratio. The hardware implementation to verify the calculated results is performed, which will be discussed in the following chapter.

CHAPTER 4

HARDWARE EXPERIMENTAL RESULTS

4.1 Hardware Test bed setup

For any system, hardware implementation is important to bring it into practicality. The validation of the obtained theoretical results is done by the hardware implementation. The design of the control circuit and the driver circuit used in the hardware are shown in the appendix. The control part, driver part and the inverter part are built and tested individually step by step before integrating all of them into a single whole system. In every stage, the parameters of the system are tested to make sure they are working according to the desired output. The hardware setup of the experiment is shown in Fig 24.
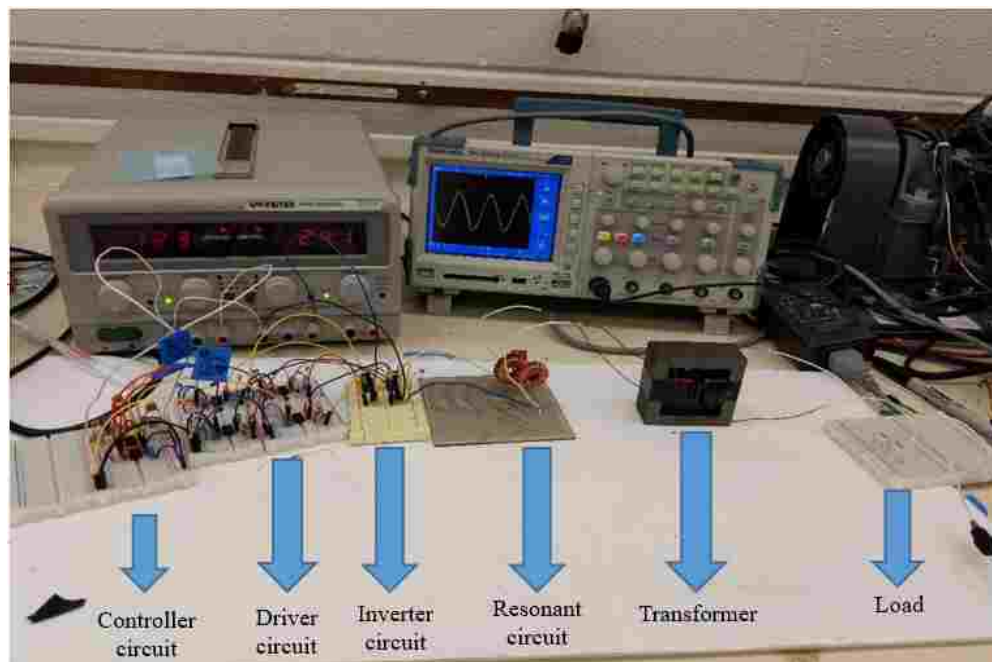

Fig 24: Hardware circuit

The hardware testing is done for the main circuit model with a low power rating. Before implementing the hardware, a simulation is done for a low power rated circuit. The specifications for low power test bed simulation are shown in table 13 below.

Table 13: Specifications for the hardware test bed

Parameter	Value
Input Voltage	12 V
Power Rating	6.25 W
Operating Frequency	20kHz
Quality Factor	5
Output voltage	24.475 V
Turns ratio	2.5

The controller and driver used for the hardware are UC-3875 Phase Shift Resonant Controller and IR2125 current limiting single channel driver respectively. UC 3875 consists of an oscillator which can operate at high frequencies and in practical applications; frequencies up to 1MHz are possible. The advantages of this controller include its protective features. It will maintain all of its outputs in active low state until a supply above 10.75 V is given.

It can also provide over current protection by latching the outputs to OFF states within 70nsec of occurrence of a fault. In this thesis, a 12 V of DC supply is given in order to energize

this controller. The controller has four outputs ABCD, out of which A, C will be in one phase and the B, D will be in a different phase. These signals from the controller are fed to the IR2125 driver circuits. There are four driver circuits in which each of the drivers sends the gate control signals for one of the four switches in the inverter. The IR2125 is a high speed MOSFET and IGBT driver, which has inbuilt over current limiting protection circuit. It is advantageous to use a driver circuit to protect the hardware involved in the system.

Using the specifications in table 13, the theoretical values for the test bed are calculated. The same equations used for calculating the system parameters in 5KW model are used for the low power circuit calculations. All the calculated values obtained for the hardware set up are shown in table 14.

Table 14: Calculated values for the hardware test bed

Parameter	Value
Voltage across the Capacitor	60 V (rms), 84.85 V (Peak)
Voltage across the Inductor	61.188 V (rms), 86.533 V (peak)
Value of Inductance	0.95 mH
Value of Capacitance	0.069 μF
Total Input Current	0.5226 A (rms) , 0.739 (peak)
Current through the Inductor	0.512 A (rms) , 0.724 A (peak)
Current through the Capacitor	0.5226 A (rms) , 0.739 (peak)

4.2 Simulation test results for hardware specifications

Fig 25 shows the whole image of the simulation system implementation of low power circuit.
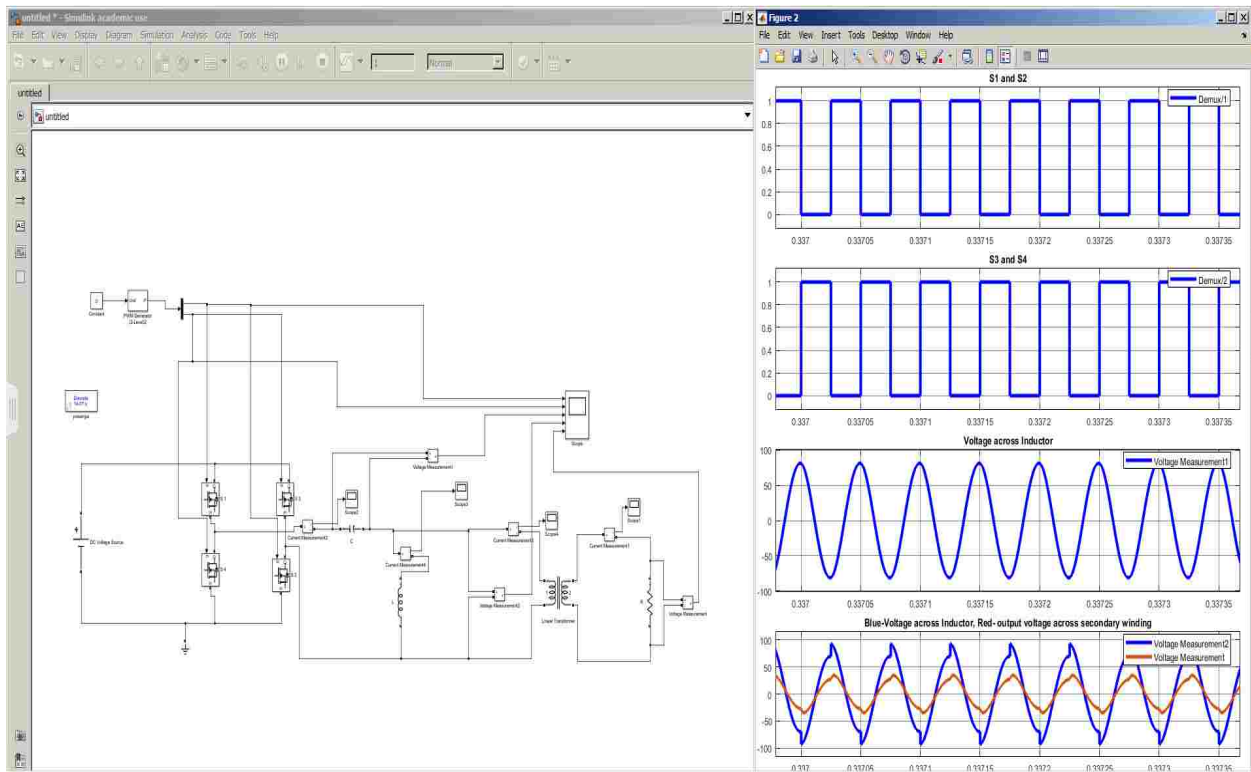
Fig 25: Simulation system for low power circuit

The simulation output waveforms for the implemented hardware model are shown below in the following figures.

Output of inverter
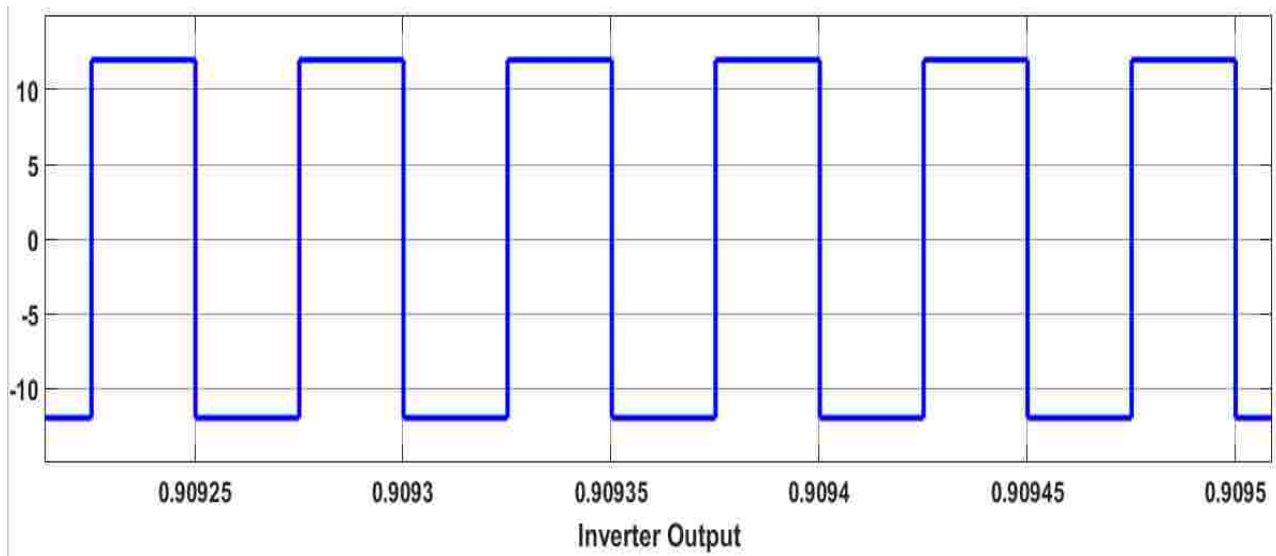
Fig 26: Inverter simulation result of low power circuit

Capacitor Voltage
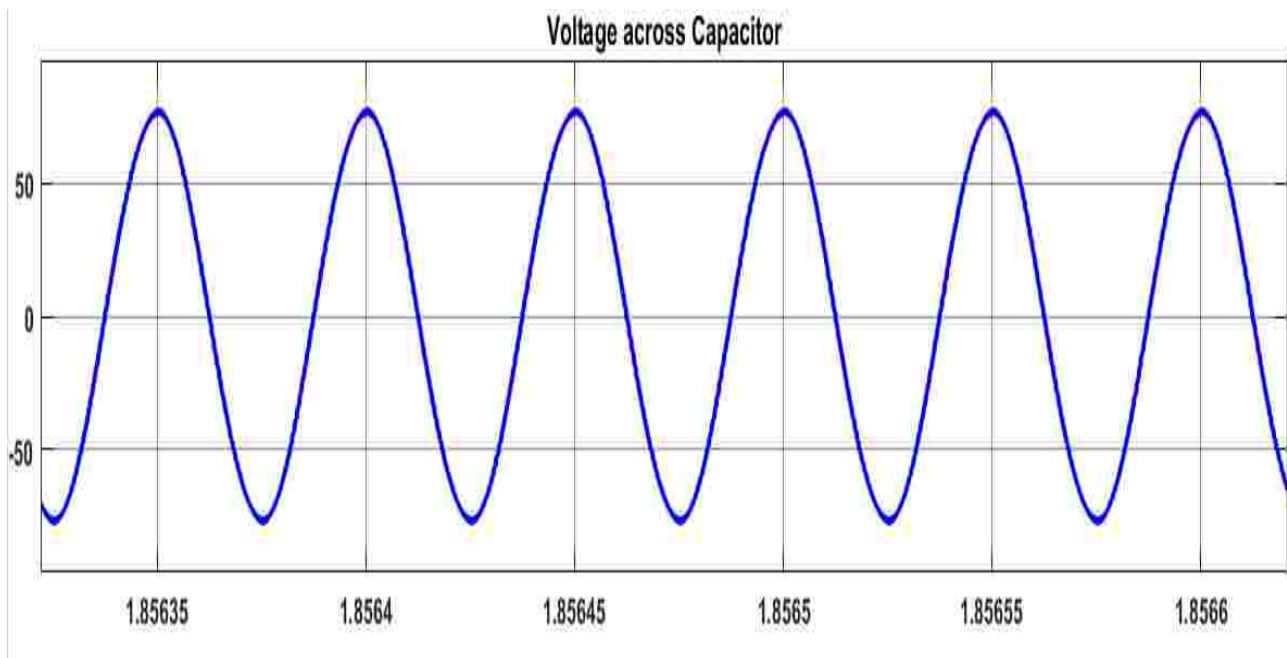
Fig 27: Simulation result of voltage across Capacitor for low power circuit

Inductor Voltage

Fig 28: Simulation result of voltage across Inductor for low power circuit

Input Current
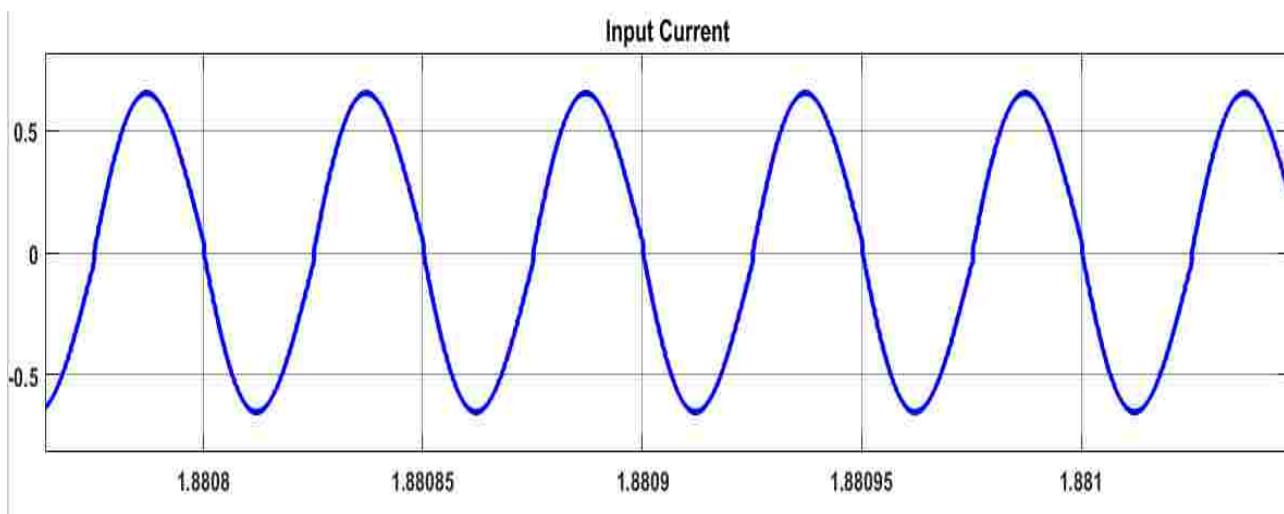
Fig 29: Simulation result of Input Current for low power circuit

Inductor Current
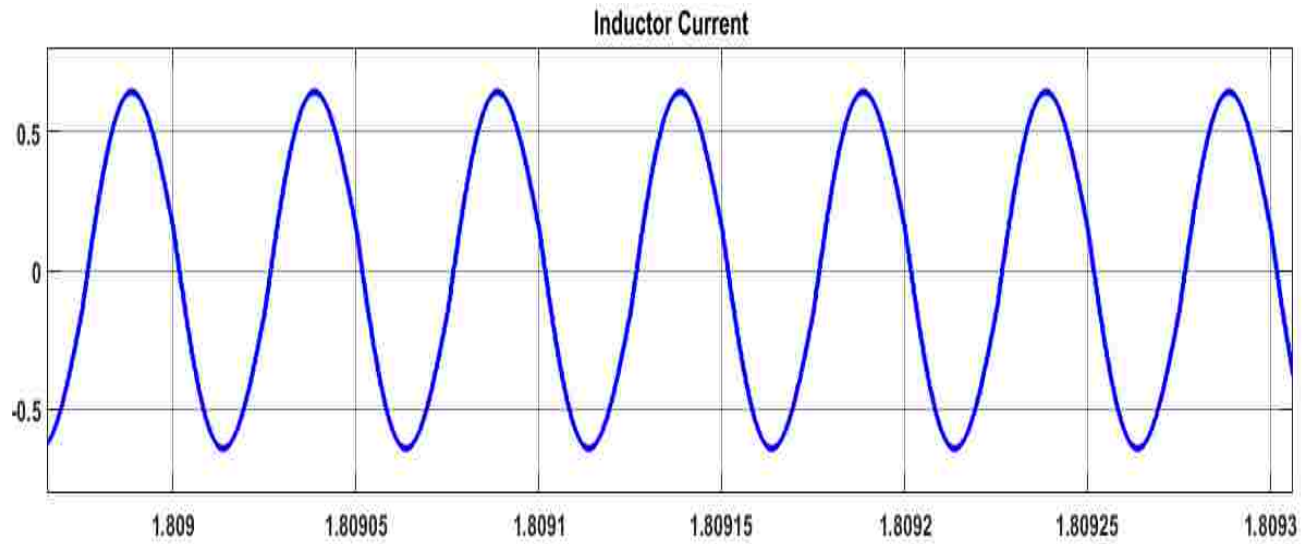
Fig 30: Simulation result of Inductor Current for low power circuit

Output Voltage across secondary Winding
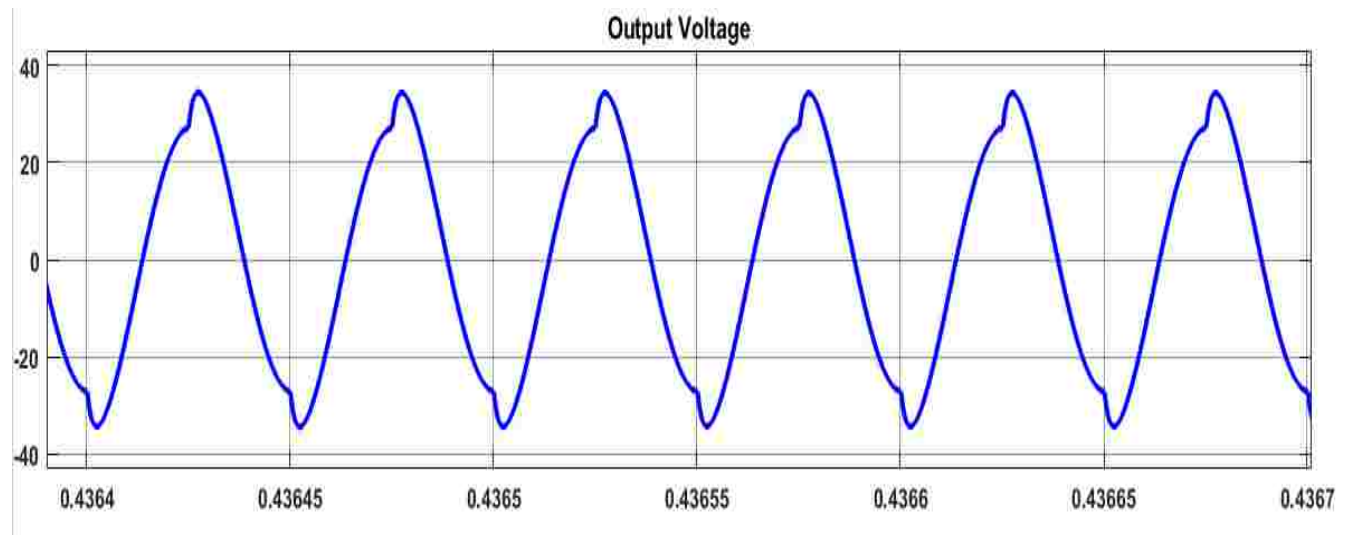
Fig 31: Simulation result of output voltage across secondary winding for low power circuit
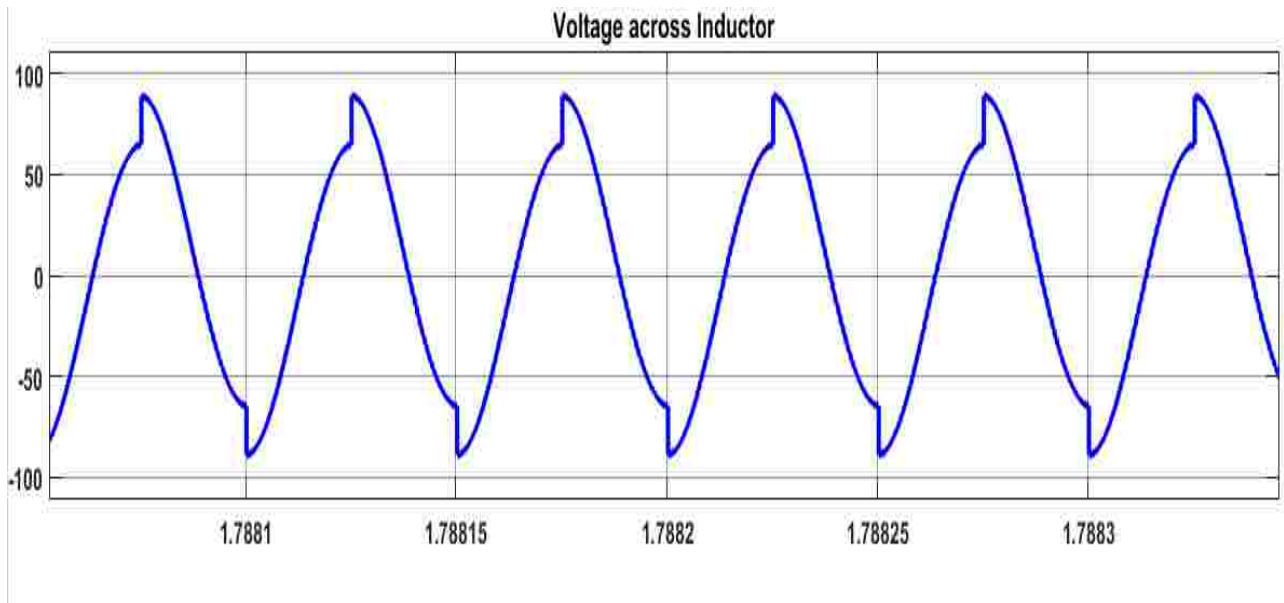
The simulation results are observed to be close to the theoretical calculations. Table 15 shows the comparison of the theoretical calculations and the simulation results for the low power test bed specifications.

Table 15. Comparison of calculated values and simulation results for low power test bed

Parameter	Theoretically Calculated Value	Value obtained from the simulation
Voltage across Inductor	61.188 V (rms) 86.53 V (peak)	87.5 V (peak)
Voltage across Capacitor	60 V (rms) 84.85 V (peak)	77.1 V (peak)
Input Current	0.5226 A (rms) 0.739 A (peak)	0.704 A (peak)
Current through Inductor	0.512 A (rms) 0.724 A (peak)	0.643 A (peak)
Output Voltage on the secondary side	24.475 V (rms) 34.613 V (peak)	34.44 V (peak)

From the above results we can conclude that the theoretical calculations are verified by the simulation results for the low power test bed.

Further, the experiment is performed for the main circuit with a 6.5 W power rating. The control circuit and the driver circuit are given 12 volts supply to energize them. The main circuit is supplied with 12V, and the outputs are verified with the theoretical calculations. In the theoretical calculations, the peak voltages across the resonant capacitor and the resonant inductor for the hardware circuit are obtained as 84.45 V and 86.53 V respectively. Fig 30 and Fig 31 show the hardware experiment output waveforms for the voltage across the resonant inductor and voltage across the resonant capacitor respectively.
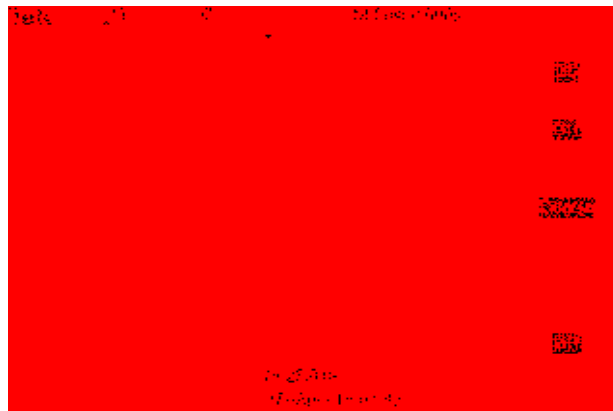
Fig 32: Hardware output for voltage across Capacitor without transmission core
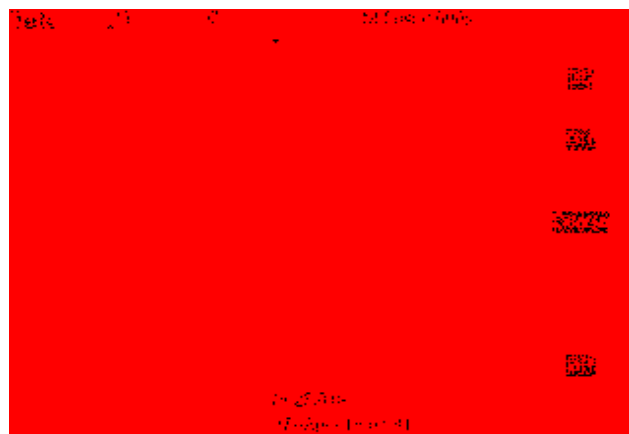
Fig 33: Hardware output for voltage across inductor without transmission core

Through the hardware, the peak voltages across the capacitor and inductor are obtained as 68 V and 84 V respectively, which are close to the theoretical values. This proves that the resonant capacitor and the resonant inductor in the hardware are validating the outputs obtained from the theoretical calculations. The test for the hardware is performed for turns ratios of 2.5 and 1. For both cases, no load test, 10% load test, 30% load test and 50% load test are performed. The distance between the transmitter and receiver is varied from 0cm to 8cm and the variation of the output voltage is noted. The results for different load tests and the output voltage variations are shown in the following section. The output voltage values for different distances are listed in the tables. Graphs are plotted between the output voltage and the distance between the transmitter and receiver to examine the variation of the output voltage with respect to the change in distance between the transmitter and receiver.

Case 1: No load test for turns ratio = 1:

Table 16: Output voltages for 1 turns ratio at no load

No load test, turns ratio = 1	
Distance between transmitter and receiver in cm	Output Voltage (V)(peak)
0	38
1	6
2	3.5
3	1.75
4	1
5	0.5
6	0.4
7	0.3
8	0.2

Fig 34: Graph across output voltage and distance for turns ratio = 1, at no load

Case 2: 10% load test for turns ratio = 1:

Table 17: Output voltages for 1 turns ratio at 10% load

10% load test, turns ratio = 1	
Distance between transmitter and receiver in cm	Output Voltage (V)(peak)
0	45
1	6.5
2	3.75
3	2
4	1
5	0.6
6	0.4
7	0.3
8	0.2

Fig 35: Graph across output voltage and distance for turns ratio = 1, at 10% load

Case 3: 30% load test for turns ratio = 1:

Table 18: Output voltages for 1 turns ratio at 30% load

30% load test, turns ratio = 1	
Distance between transmitter and receiver in cm	Output Voltage (V)(peak)
0	44
1	6.5
2	3.5
3	1.5
4	1
5	0.6
6	0.4
7	0.25
8	0.2

Fig 36: Graph across output voltage and distance for turns ratio = 1, at 30% load

Case 4: 50% load test for turns ratio = 1:

Table 19: Output voltages for 1 turns ratio at 50% load

50% load test, turns ratio = 1	
Distance between transmitter and receiver in cm	Output Voltage (V)(peak)
0	38
1	6
2	3
3	1.5
4	1
5	0.6
6	0.4
7	0.2
8	0.15

Fig 37: Graph across output voltage and distance for turns ratio = 1, at 50% load

Case 5: no load test for turns ratio = 2.5:

Table 20: Output voltages for 2.5 turns ratio at no load

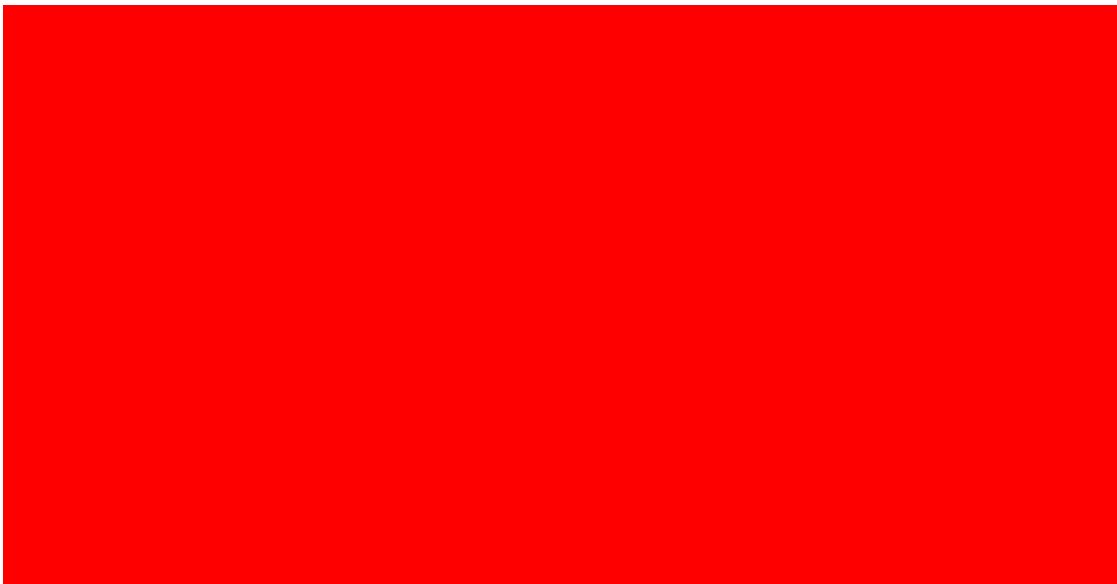| No load test, turns ratio = 2.5	
Distance between transmitter and receiver in cm	Output Voltage (V)(peak)
0	12
1	2.5
2	1.5
3	0.7
4	0.35
5	0.2
6	0.12
7	0.1
8	0.08

Fig 38: Graph across output voltage and distance for turns ratio = 2.5, at no load

Case 6: 10% load test for turns ratio = 2.5:

Table 21: Output voltages for 2.5 turns ratio at 10% load

10% load test, turns ratio = 2.5	
Distance between transmitter and receiver in cm	Output Voltage (V)(peak)
0	15
1	3
2	1.75
3	0.7
4	0.4
5	0.2
6	0.15
7	0.1
8	0.07

Fig 39: Graph across output voltage and distance for turns ratio = 2.5, at 10% load

Case 7: 30% load test for turns ratio = 2.5:

Table 22: Output voltages for 2.5 turns ratio at 30% load

30% load test, turns ratio = 2.5	
Distance between transmitter and receiver in cm	Output Voltage (V)
0	15
1	3
2	1.5
3	0.75
4	0.4
5	0.25
6	0.15
7	0.1
8	0.08

Fig 40: Graph across output voltage and distance for turns ratio = 2.5, at 30% load

Case 7: 50% load test for turns ratio = 2.5:

Table 23: Output voltages for 2.5 turns ratio at 50% load

50% load test turns ratio = 2.5	
Distance between transmitter and receiver in cm	Output Voltage (V)
0	13
1	2.5
2	1.25
3	0.6
4	0.4
5	0.25
6	0.15
7	0.1
8	0.075

Fig 41: Graph across output voltage and distance for turns ratio = 2.5, at 50% load

From the above figures it can be seen that the system worked well at the different load conditions. Although the output voltage on the secondary side decreased with an increase in the coupling distance, there was considerable output induced across the secondary terminals at all the load conditions. When the primary and secondary are placed close to each other, and the load is increased gradually, there was no significant drastic drop observed in the output voltage on the secondary side. The voltage obtained across the primary terminals or across the resonant inductor is observed to be very close to the theoretical calculations and simulation results of the low power circuit. Hence, the hardware results validated the results obtained from the theory and simulations.

4.3 Hard ware limitation:

For all the tests performed at different load conditions, even though the system performance was satisfactory, the voltages on the secondary side are observed to be reduced to nearly half of the desired value obtained in the theoretical calculations. Also, a drastic drop in the output voltage was observed in all the cases when the distance between the coils is varied from 0cm to 3cm. Although the voltages obtained on the secondary side are not very close to the desired values, the output of this system can be increased further if the hardware test bed is implemented on the PCB (printed circuit board). PCB implementation can help produce results with fewer losses and less damage caused due to wiring issues. This can also help in reducing the troubleshooting time by further improving system performance.

CHAPTER 5

CONCLUSION AND FUTURE WORK

6.1 Conclusion

A 5KW Inductive power transfer system for electric vehicle applications in MVDC networks is designed and analyzed. According to the specifications of the system, the design is observed to show good performance at a turns ratio of 2.5. When the turns ratio is decreased beyond 2.5, the Quality factor of the system fell below the desired value. Also, the voltage across the resonant Inductor and Capacitor declined. If the Quality factor of the system and the voltage on the transmitting side decreases, the performance of the system drops as the transmitter's ability to transfer energy onto the secondary side also drops. The coupling distance also cannot be varied to a long range with a decrease in performance. Hence, it can be concluded that this proposed system, when designed with a turns ratio of 2.5, produced the desired results validated by simulation results, so this system is useful for practical applications.

6.2 Future Work

Since hardware tests were done on a low-power test bed, future work should focus on implementing the high-power hardware testbed and testing its performance.

REFERENCES

1. Mi, Chris, and M. Abul Masrur. *Hybrid electric vehicles: principles and applications with practical perspectives*. John Wiley & Sons, 2017.

2. Morris C. The dynamic road ahead: Utah State University builds the nation's most advanced test facility for dynamic wireless charging. Charged EVs: <chargedevs.com>; Nov/Dec 2014. p. 82–7.

3. S. J. Gerssen-Gondelach and A. P. C. Faaij, "Performance of batteries for electric vehicles on short and longer term," J. Power Sour., vol. 212, pp. 111–129, Aug. 2012.

4. V. Etacheri, R. Marom, R. Elazari, G. Salitra, and D. Aurbach, "Chal- lenges in the development of advanced Li-ion batteries: A review," Energy Environ. Sci., vol. 4, no. 9, pp. 3243–3262, 2011.

5. M.A. Rodriguez-Otero and E. O'Neill-Carrillo. "Efficient Home Appliances for a Future DC Residence". In: Energy 2030 Conference, 2008. ENERGY 2008. IEEE. Nov. 2008, pp. 1–6.

6. Stieneker, Marco, and Rik W. De Doncker. "Medium-voltage DC distribution grids in urban areas." *2016 IEEE 7th International Symposium on Power Electronics for Distributed Generation Systems (PEDG)*. IEEE, 2016.

7. Reed, Gregory F., et al. "Ship to grid: Medium-voltage DC concepts in theory and practice." *IEEE Power and Energy Magazine* 10.6 (2012): 70-79.

8. F. Mura and R. W. De Doncker. "Design aspects of a medium-voltage direct current (MVDC) grid for a university campus". In: Power Electronics and ECCE Asia (ICPE ECCE), 2011 IEEE 8th International Conference on. May 2011, pp. 2359–2366.

9. M. Stieneker, J. Butz, S. Rabiee, H. Stagge, and R. W. D. Doncker. "Medium-Voltage DC Research Grid Aachen". In: International ETG Congress 2015; Die Energiewende - Blueprints for the new energy age; Proceedings of. Nov. 2015, pp. 1–7.

10. Porter, Suzanne Foster, et al. "Reviving the War of Currents: Opportunities to Save Energy with DC Distribution in Commercial Buildings." (2014).

11. Bathurst, Graeme, George Hwang, and Lalit Tejwani. "MVDC-the new technology for distribution networks." (2015): 027-5.

12. Rim, Chun T., and Chris Mi. *Wireless power transfer for electric vehicles and mobile devices*. John Wiley & Sons, 2017.

13. N. Shinohara, Y. Kubo, and H. Tonomura, "Wireless Charging for Electric Vehicle with Microwaves," in Proc. of International Electric Drives Production Conference (EDPC), Nuremberg, German, Oct. 2013.

14. Tang, Qinghui, et al. "Communication scheduling to minimize thermal effects of implanted biosensor networks in homogeneous tissue." *IEEE Transactions on Biomedical Engineering* 52.7 (2005): 1285-1294.

15. Popovic, Zoya. "Far-field wireless power delivery and power management for low-power sensors." *2013 IEEE Wireless Power Transfer (WPT)*. IEEE, 2013.

16. Kim, Han-Joon, et al. "Review of near-field wireless power and communication for biomedical applications." *IEEE Access* 5 (2017): 21264-21285.

17. J. I. Agbinya et al., ''Size and characteristics of the 'cone of silence' in near-field magnetic induction communications,'' in Proc. MiLCIS, Nov. 2009, pp. 1–4

18. Lu, Xiao, et al. "Wireless charging technologies: Fundamentals, standards, and network applications." *IEEE Communications Surveys & Tutorials* 18.2 (2015): 1413-1452.

19. Pande, Vishal V., et al. "Wireless power transmission using resonance inductive coupling." *International Journal of Engineering Research and Applications* 4.4 (2014).

20. Dai, Jiejian, and Daniel C. Ludois. "A survey of wireless power transfer and a critical comparison of inductive and capacitive coupling for small gap applications." *IEEE Transactions on Power Electronics* 30.11 (2015): 6017-6029.

21. Waffenschmidt, E., "Wireless power for mobile devices," Telecommunications Energy Conference (INTELEC), 2011 IEEE 33rd International , vol., no., pp.1,9, 9-13 Oct. 2011

22. Rao[1], TS Chandrasekar, and K. Geetha. "Categories, standards and recent trends in wireless power transfer: A survey." *Indian Journal of Science and Technology* 9 (2016): 20.

23. Wheeler, L. P. "II—Tesla's contribution to high frequency." *Electrical Engineering* 62.8 (1943): 355-357.

24. Marincic, A. S. "Nikola tesla and the wireless transmission of energy." *IEEE Transactions on Power Apparatus and Systems*10 (1982): 4064-4068.

25. Shidujaman, Mohammad, Hooman Samani, and Mohammad Arif. "Wireless power transmission trends." *2014 International Conference on Informatics, Electronics & Vision (ICIEV)*. IEEE, 2014.

26. Hou, Chung-Chuan, et al. "Resonant and non-resonant inductive power transfer systems based on planar spiral coils." *2017 IEEE 3rd International Future Energy Electronics Conference and ECCE Asia (IFEEC 2017-ECCE Asia)*. IEEE, 2017.

27. Kim, J., D-H. Kim, and Y-J. Park. "Effective magnetic resonant wireless power transfer system over medium range using an intermediate resonant coil of two loops." *2015 IEEE-APS Topical Conference on Antennas and Propagation in Wireless Communications (APWC)*. IEEE, 2015.

28. Han, Sangwook, and David D. Wentzloff. "Wireless power transfer using resonant inductive coupling for 3D integrated ICs." *2010 IEEE International 3D Systems Integration Conference (3DIC)*. IEEE, 2010.

29. Kurs, Andre, et al. "Wireless power transfer via strongly coupled magnetic resonances." science 317.5834 (2007): 83-86.

30. Jay, Rajiv, and Samuel Palermo. "Resonant coupling analysis for a two-coil wireless power transfer system." *2014 IEEE Dallas Circuits and Systems Conference (DCAS)*. IEEE, 2014.

31. Barman, Surajit Das, et al. "Wireless powering by magnetic resonant coupling: Recent trends in wireless power transfer system and its applications." *Renewable and Sustainable energy reviews* 51 (2015): 1525-1552.

32. Alexander, Charles K., and Matthew no Sadiku. "Electric circuits." *Transformation* 135 (2000): 4-5.

33. Jiang, Chaoqiang, et al. "An overview of resonant circuits for wireless power transfer." *Energies* 10.7 (2017): 894.

34. A. Kurs, A. Karalis, R. Moffatt, J. D. Joannopoulos, P. Fisher, and M. Soljacic, "Wireless Power Transfer via Strongly Coupled Magnetic Resonances," Science, vol. 317, no. 5834, pp. 83-86, June 2007.

35. Lopez, Toni, and Reinhold Elferich. "Method for the analysis of power MOSFET losses in a synchronous buck converter." *2006 12th International Power Electronics and Motion Control Conference*. IEEE, 2006.

36. Shen, Z. John, et al. "Power MOSFET switching loss analysis: A new insight." *Conference Record of the 2006 IEEE Industry Applications Conference Forty-First IAS Annual Meeting*. Vol. 3. IEEE, 2006.

37. C. S. Wang, G. A. Covic, and O. H. Stielau, "Power Transfer Capability and Bifurcation Phenomena of Loosely Coupled Inductive Power Transfer Systems," IEEE Trans. Ind. Electron., vol. 51, no. 1, pp. 148-157, Feb. 2004.
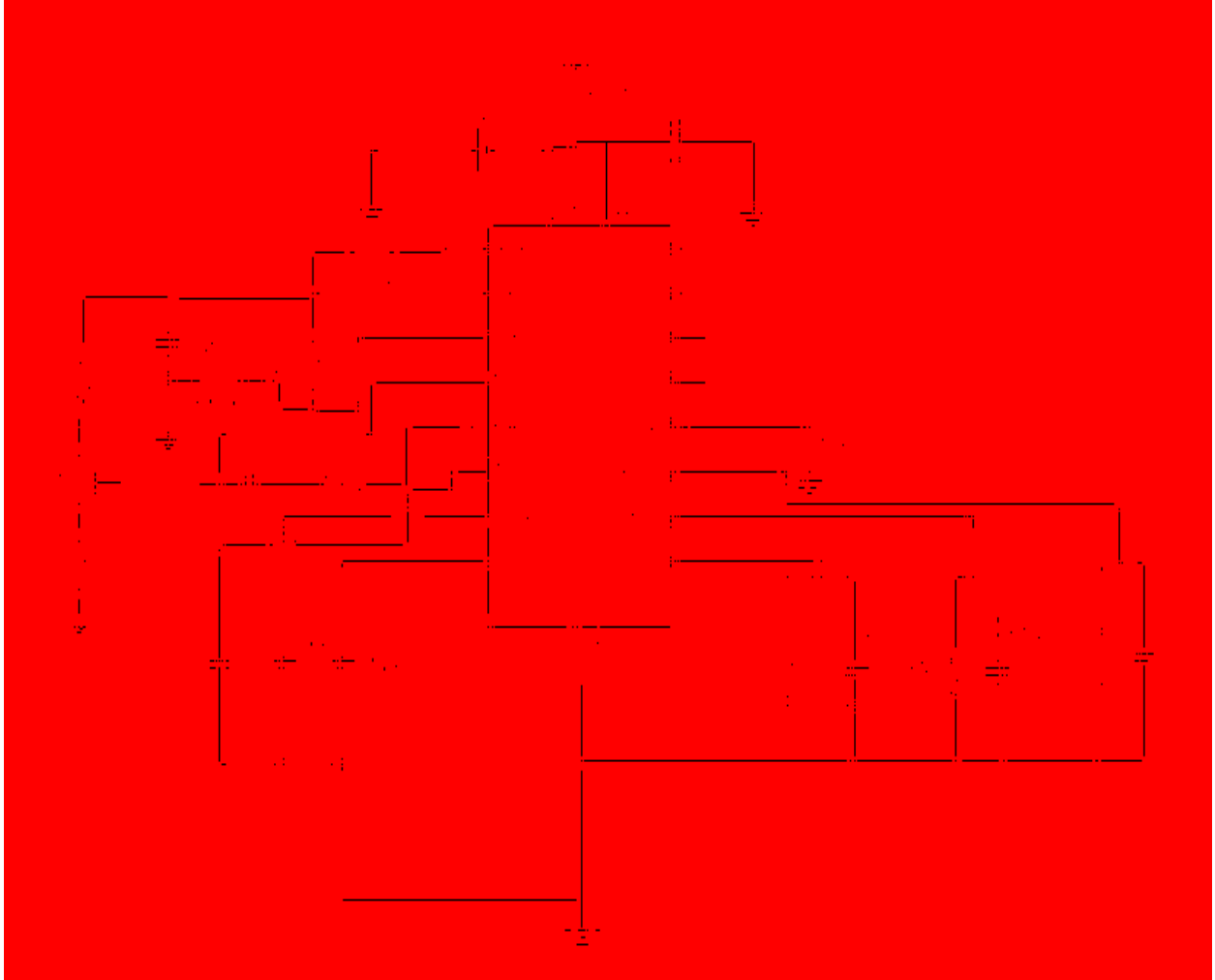
APPENDIX

UC-3875 (Controller)
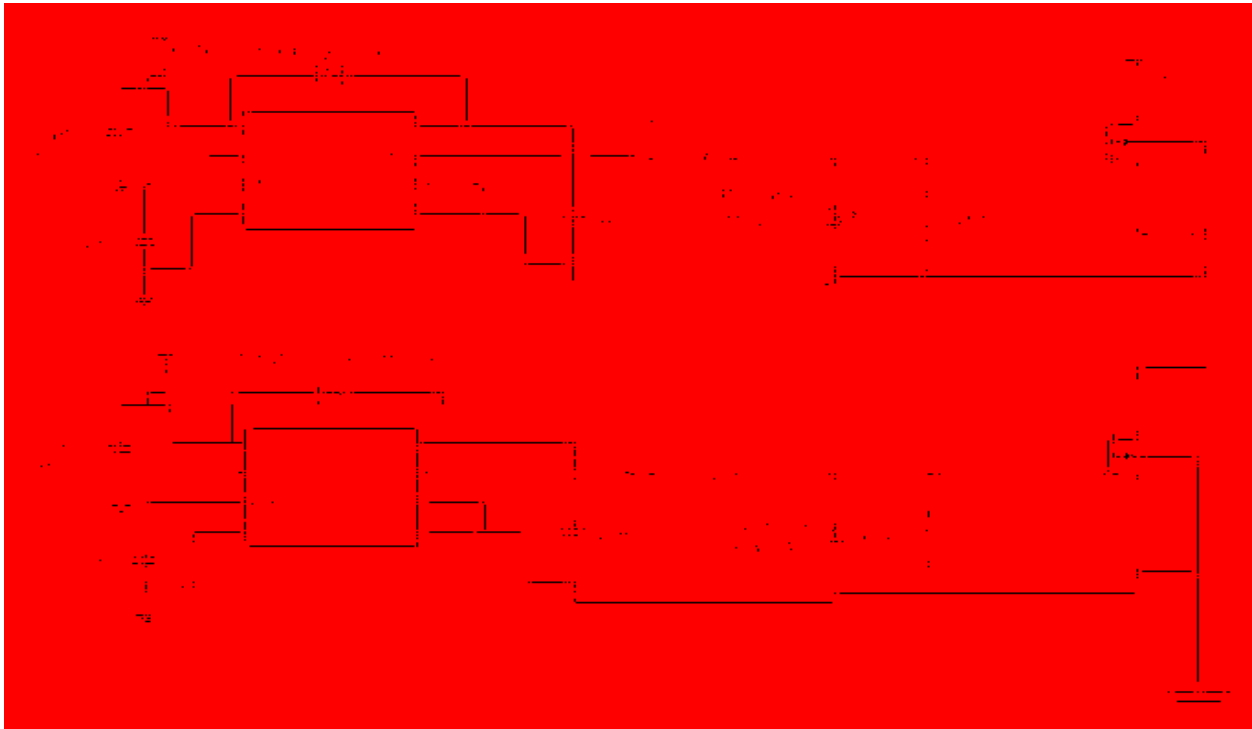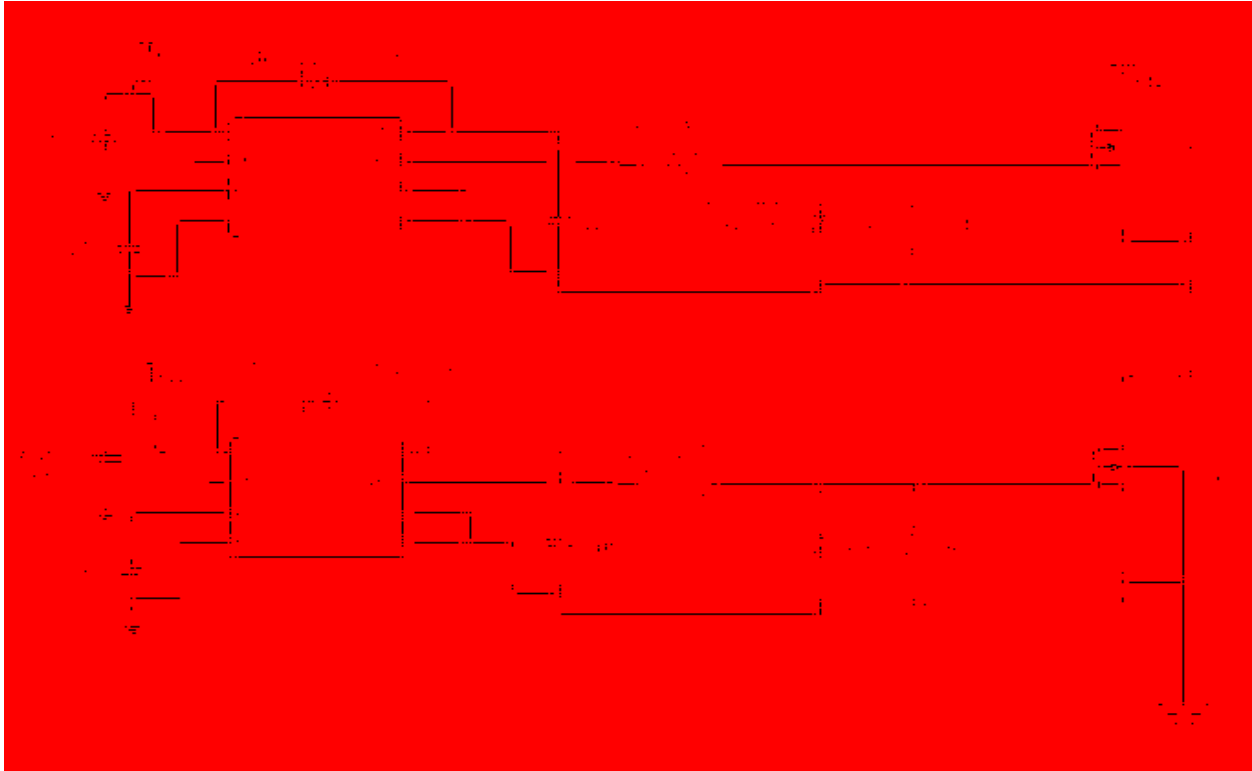

Fig 42: Controller Circuit

IR2125 (Driver Circuit)

Fig 43: Driver Circuit

VITA

Sarika Reddy Daida
231 Kaufmann Hall
ECE Department
Old Dominion University
Norfolk, VA 23529

Education

Old Dominion University, Norfolk, VA	Aug 2017-July 2019
Master of Science in Electrical and Computer Engineering	
Jawaharlal Nehru Technological University, Hyderabad, India.	Aug 2012-May 2016
Bachelor of Technology in Electrical and Electronics Engineering	

Work Experience

Old dominion university, Norfolk, VA	
Graduate Research Assistant	Aug 2017- Present
Graduate Teaching Assistant	Aug 2017-Present
Bharat Heavy Electricals Limited, Hyderabad, India.	
Electrical Engineering Intern	April 2015- July 2015

Technical projects

Old Dominion University, Norfolk, VA	
Resonant Inductive Wireless Power Transfer system	Aug 2017- Present
JNTU, India	
Super Capacitors and battery power management for hybrid vehicle	Aug 2015- Dec 2015
JNTU, India	
Power theft monitoring systems	Jan 2016- May 2016